

See discussions, stats, and author profiles for this publication at: <https://www.researchgate.net/publication/343653135>

How Does the Quasi-Biennial Oscillation Affect the Boreal Winter Tropospheric Circulation in CMIP5/6 Models?

Article in *Journal of Climate* · August 2020

DOI: 10.1175/JCLI-D-20-0024.1

CITATIONS

2

READS

110

3 authors:



Jian Rao

Hebrew University of Jerusalem

61 PUBLICATIONS 431 CITATIONS

[SEE PROFILE](#)



Chaim I. Garfinkel

Hebrew University of Jerusalem

102 PUBLICATIONS 2,480 CITATIONS

[SEE PROFILE](#)



Ian White

Hebrew University of Jerusalem

34 PUBLICATIONS 577 CITATIONS

[SEE PROFILE](#)

Some of the authors of this publication are also working on these related projects:



Stratospheric Predictability [View project](#)



Seasonal evolution of the QBO-induced wave forcing and circulation anomalies in the Northern winter stratosphere [View project](#)

How Does the Quasi-Biennial Oscillation Affect the Boreal Winter Tropospheric Circulation in CMIP5/6 Models?

JIAN RAO

Key Laboratory of Meteorological Disaster, Ministry of Education/Joint International Research Laboratory of Climate and Environment Change/Collaborative Innovation Center on Forecast and Evaluation of Meteorological Disasters, Nanjing University of Information Science and Technology, Nanjing, China, and Fredy and Nadine Herrmann Institute of Earth Sciences, The Hebrew University of Jerusalem, Givat Ram, Jerusalem, Israel

CHAIM I. GARFINKEL AND IAN P. WHITE

Fredy and Nadine Herrmann Institute of Earth Sciences, The Hebrew University of Jerusalem, Givat Ram, Jerusalem, Israel

(Manuscript received 15 January 2020, in final form 29 July 2020)

ABSTRACT: Using 17 CMIP5 and CMIP6 models with a spontaneously generated quasi-biennial oscillation (QBO)-like phenomenon, this study explores and evaluates three dynamical pathways for impacts of the QBO on the troposphere: 1) the Holtan–Tan (HT) effect on the stratospheric polar vortex and the northern annular mode (NAM), 2) the subtropical zonal wind downward arching over the Pacific, and 3) changes in local convection over the Maritime Continent and Indo-Pacific Ocean. More than half of the models can reproduce at least one of the three pathways, but few models can reproduce all of the three routes. First, seven models are able to simulate a weakened polar vortex during easterly QBO (EQBO) winters, in agreement with the HT effect in the reanalysis. However, the weakened polar vortex response during EQBO winters is underestimated or not present at all in other models, and hence the chain for QBO, vortex, and tropospheric NAM/AO is not simulated. For the second pathway associated with the downward arching of the QBO winds, 10 models simulate an inconsistent extratropical easterly anomaly center over 20°–40°N in the Pacific sector during EQBO, and hence the negative relative vorticity anomalies poleward of the easterly center is not present in those models, leading to no consensus on the height response over the North Pacific between those models and the reanalysis. However, the other seven models do capture this effect. The third pathway is only observed in the Indo-Pacific Ocean, where the strong climatological deep convection and the warm pool are situated. Seven models can simulate the convection anomalies associated with the QBO over the Maritime Continent, which is likely caused by the near-tropopause low buoyancy frequency anomalies. No robust relationship between the QBO and El Niño–Southern Oscillation (ENSO) events can be established using the JRA55 reanalysis, and 10 models consistently confirm little modulation of the ocean basinwide Walker circulation and ENSO events by the QBO.

KEYWORDS: Northern Hemisphere; Stratosphere-troposphere coupling; Model evaluation/performance; Quasi-biennial oscillation

1. Introduction

The quasi-biennial oscillation (QBO) is the most cyclic dynamical phenomenon in the atmosphere not related to solar radiation, and manifests as downward descending westerly and easterly momentum from the upper stratosphere to the tropopause over the equator with a periodicity of ~28 months (Baldwin et al. 2001). Recently there has been a rapid increase in the number of models that are capable of simulating a spontaneous QBO, and sufficiently fine vertical resolution [e.g., <750 m–1 km in the tropical stratosphere; see Fig. 4 in Butchart et al. (2018)] in the lower stratosphere has been identified as an important ingredient for most of those models [e.g., L60CAM in Richter et al. (2014); GISS-E2 in Rind et al. (2014); MRI-ESM2.0 in Naoe and Yoshida (2019); HadGEM3

in Andrews et al. (2019); and BCC-AGCM in Lu et al. (2020)]. At least three different mechanisms have been proposed to explain how the QBO can affect tropospheric and surface climate (to be discussed shortly). Since many state-of-the-art models can now reproduce a QBO-like circulation in the tropical stratosphere, a more robust understanding of these mechanisms can be attained by intercomparing models (e.g., extratropical and tropospheric impacts, and their changes in the future).

The early study by Holton and Tan (1980) found that the QBO can modify the zero-wind line whereby the width of the extratropical waveguide is changed for upward-propagating planetary waves from the troposphere. Specifically, alternate QBO phases lead to a shift in the latitudes of the zero-wind line at 50 hPa from the equator to subtropics, and therefore the region into which tropospheric planetary waves are permitted to propagate is dependent on QBO phase (Baldwin et al. 2001; Anstey and Shepherd 2014; Andrews et al. 2019). The QBO subsequently can impact the Northern Hemisphere (NH) winter stratospheric polar vortex, which tends to be weaker and warmer during the easterly phase of QBO at 30–50 hPa

Supplemental information related to this paper is available at the Journals Online website: <https://doi.org/10.1175/JCLI-D-20-0024.s1>.

Corresponding author: Jian Rao, jian.rao@mail.huji.ac.il

DOI: 10.1175/JCLI-D-20-0024.1

© 2020 American Meteorological Society. For information regarding reuse of this content and general copyright information, consult the AMS Copyright Policy (www.ametsoc.org/PUBSReuseLicenses).

(Holton and Tan 1980; Baldwin and Tung 1994; Baldwin et al. 2001; Ruzmaikin et al. 2005; Marshall and Scaife 2009). This is the so-called Holton–Tan (HT) relationship, although the mechanism proposed by HT may not explain the entirety of the polar stratospheric response (Garfinkel et al. 2012; Watson and Gray 2014; White et al. 2015). Variability of the NH stratospheric polar vortex may impact European surface climate, the Siberian high, and the East Asian winter monsoon through the projected northern annular mode or Arctic Oscillation (NAM/AO) (Thompson and Wallace 2000; Gong et al. 2001; Baldwin and Dunkerton 1999; Scaife et al. 2005), which can bridge the tropical QBO and the extratropical climate variations [Marshall and Scaife 2009; also see the review papers by Baldwin et al. (2001) and Anstey and Shepherd (2014)]. The QBO is potentially a source of predictability for the NH winter weather and climate (Garfinkel et al. 2018; Marshall and Scaife 2009).

Second, QBO winds appear to arch poleward and downward from the tropical lower stratosphere to near 20°N (Crooks and Gray 2005), with the effect particularly pronounced in the Pacific sector (Garfinkel and Hartmann 2011a,b). By using models with different complexities (i.e., the GFDL dry model and WACCM), Garfinkel and Hartmann (2011a,b) demonstrated that the QBO-induced meridional circulation causes zonal wind anomalies in the subtropical troposphere that extend from the equatorial stratosphere. In the presence of extratropical eddies, the zonal wind anomalies are intensified and extend downward to the surface. This meridional circulation is also associated with equatorward Eliassen–Palm (EP) flux anomalies in the lower stratosphere when easterly winds are present in the tropical lower stratosphere, an effect not expected from the HT mechanism (Garfinkel and Hartmann 2011a; Garfinkel et al. 2012; Seo et al. 2013; White et al. 2015; Rao et al. 2020). Naoe and Yoshida (2019) modeled in MRI-ESM2.0 enhanced meridional potential vorticity (PV) gradients (positive q_ϕ anomalies) spreading from the subtropical lower stratosphere due to downward-arching zonal wind anomalies (also see White et al. 2015, 2016). The net effect is that the QBO phase with easterlies in the tropical lower stratosphere is associated with a poleward shifted jet in the North Pacific sector of the troposphere due to the QBO's direct meridional circulation cell (Randel et al. 1999; Garfinkel and Hartmann 2011a,b).

Third, the QBO-induced zonal-mean direct meridional circulation cell changes the temperature vertical profile in the equatorial upper troposphere and lower stratosphere, so the atmospheric stability is also changed. In this way, the QBO may directly influence tropical deep convection and upper tropospheric divergence, which provides a Rossby wave source to excite related teleconnections spanning the tropics and extratropics (Collimore et al. 2003; Garfinkel and Hartmann 2011b; Liess and Geller 2012; Nie and Sobel 2015; Gray et al. 2018).

Due to the limited time span of the observational QBO record, it is still not clear which of these mechanisms dominates. It is likely that different mechanisms are more important for different regions in the troposphere. In addition, further work is needed to clarify the details behind each of these different possibilities. The long historical runs of different models from

phases 5 and 6 of the Coupled Model Intercomparison Project–(CMIP5 and CMIP6, jointly CMIP5/6; Taylor et al. 2012; Eyring et al. 2016) provide us an opportunity to separate the three dynamical pathways. The Atmospheric Model Intercomparison Project (AMIP)-type simulations from the QBO initiative (QBOi) models (e.g., Bushell et al. 2020) in previous studies show a less robust and less consistent EQBO minus WQBO composite in the extratropics (Butchart et al. 2018; Naoe and Yoshida 2019). Using 16 CMIP5/6 models, Rao et al. (2020) have recently evaluated the QBO and its influence on the NH stratospheric polar vortex. We build on those results here and, using the same model data, systematically explore the different routes bridging QBO and the extratropical tropospheric circulation.

The overarching question we seek to answer is this: What is the relative impact of these three pathways for the influence of the QBO on surface climate? This overarching question can be divided into three more targeted questions: 1) Can all the CMIP5/6 models with QBO-like signals reproduce the three dynamical pathways for the troposphere? 2) Which dynamical pathways are more important for East Asian and North Pacific climate? What can explain the intermodel spread with regards to models (i.e., which simulate a surface impact versus ones which do not)? 3) Are the tropical deep convection anomalies associated with QBO zonally symmetric? If not, in which tropical region is deep convection most sensitive to the QBO phase? What factors may lead to the zonal structure? The structure of the paper is arranged as below. Following the introduction, section 2 presents the multiple CMIP5/6 models and methods employed in this study. The three QBO dynamical pathways for the tropospheric circulation responses are assessed in sections 3–5, respectively, for CMIP5/6 models. The possibility of a connection between QBO and El Niño–Southern Oscillation (ENSO) is discussed in section 6. Finally, section 7 presents a summary and discussion.

2. Model datasets and methods

a. Selected CMIP5/6 models with QBO-like signals

There are at least 17 QBO-resolving models available used in this study, including 6 CMIP5 models (CESM1-WACCM, CMCC-CMS, HadGEM2-CCS, MIROC-ESM, MIROC-ESM-CHEM, MPI-ESM-MR) and 11 CMIP6 models (from BCC-CSM2-MR to UKESM1.0-LL in Table 1). Four CMIP5 models (HadGEM2-CCS, MIROC-ESM-CHEM, MIROC-ESM, MPI-ESM-MR) were also used by Kawatani and Hamilton (2013). Because some variables (e.g., outgoing longwave radiation and precipitation) are unavailable in the GEOSCCM model (Li et al. 2016), we discard this model although it is used to study the HT relationship in Rao et al. (2020). Note that the first CMIP5 model, CESM1-WACCM, cannot internally simulate the QBO, and the QBO zonal winds between 86 and 4 hPa are nudged toward the observed QBO with an approximate 28-month cycle period (Marsh et al. 2013). All the CMIP5 models have a model top at or above the 1-hPa pressure level and have at least 60 vertical levels. Historical experiments from those high-top CMIP5 models have also been widely used to explore the stratospheric sudden warming frequency and ENSO teleconnections

TABLE 1. Selected QBO-resolving CMIP5/6 models used in this study. The integration time span for CMIP5 (CMIP6) is 1850–2005 (1850–2014) in the historical run. Note that this study does not analyze the GEOSCCM model in Rao et al. (2020) due to the unavailability of some variables (e.g., outgoing longwave radiation and precipitation). We also add another two CMIP6 models, EC-Earth3-Veg and HadGEM3-GC31-LL.

| Model | Affiliation and nationality | Horizontal resolution (lat × lon) | Top (levels) | Reference |
|---------------------|---------------------------------------|--------------------------------------|-------------------------------------|----------------------------|
| CESM1-WACCM | NSF–DOE–NCAR, United States | F19 (96 × 144) | 5.1 × 10 ⁻⁶ hPa (L66) | Marsh et al. (2013) |
| CMCC-CMS | CMCC, Italy | T63 (96 × 192) | 0.01 hPa (L95) | Davini et al. (2014) |
| HadGEM2-CCS | MOHC, United Kingdom | N96 (144 × 192) | 85 km (L60) | Martin et al. (2011) |
| MIROC- ESM-CHEM | CCSR/NIES-AORI /UT- JAMSTEC, Japan | T42 (64 × 128) | 0.0036 hPa (L80) | Watanabe et al. (2011) |
| MIROC-ESM | CCSR/NIES-AORI /UT- JAMSTEC, Japan | T42 (64 × 128) | 0.0036 hPa (L80) | Watanabe et al. (2011) |
| MPI-ESM-MR | MPI, Germany | T63 (96 × 192) | 0.01 hPa (L95) | Giorgetta et al. (2013) |
| BCC-CSM2-MR | CMA-BCC, China | T106 (160 × 320) | 1.46 hPa (L46) | Wu et al. (2019) |
| CESM2-WACCM | NSF–DOE–NCAR, United States | F09 (192 × 288) | 4.5 × 10 ⁻⁶ hPa (L70) | Liu et al. (2018) |
| CNRM-CM6-1 | CNRM, France | T _L 127 (128 × 256) | 78.4 km (L91) | Voltaire et al. (2019) |
| CNRM-ESM2-1 | CNRM, France | T _L 127 (128 × 256) | 78.4 km (L91) | Séférián et al. (2016) |
| EC-Earth3 | EC-Earth Consortium, Europe | T _L 255 (256 × 512) | 0.01 hPa (L91) | Massonnet et al. (2020) |
| EC-Earth3-Veg | EC-Earth Consortium, Europe | T _L 255 (256 × 512) | 0.01 hPa (L91) | Massonnet et al. (2020) |
| HadGEM3- GC31-LL | MOHC, United Kingdom | N96 (144 × 192) | 85 km (L85) | Menary et al. (2018) |
| IPSL-CM6A-LR | IPSL, France | N96 (143 × 144) | 80 km (L79) | Dufresne et al. (2013) |
| MIROC6 | CCSR/NIES-AORI /UT- JAMSTEC, Japan | T85 (128 × 258) | 0.004 hPa (L81) | Tatebe et al. (2019) |
| MRI-ESM2.0 | JMA-MRI, Japan | T _L 159 (160 × 320) | 0.01 hPa (L80) | Yukimoto et al. (2019) |
| UKESM1.0-LL | MOHC/NCAS, United Kingdom | N96 (144 × 192) | 85 km (L85) | Kuhlbrodt et al. (2018) |

(Charlton-Perez et al. 2013; Hurwitz et al. 2014; Calvo et al. 2017; Rao et al. 2019). Historical experiments are forced by time-varying, externally imposed conditions that are based on observations. Both naturally forced changes (e.g., solar variability and volcanic aerosols) and changes due to human activities (e.g., greenhouse gases, aerosols, and land use) are incorporated.

Nearly 30 CMIP6 models, to our best knowledge, released historical experiments by the time we finished downloading data for this study (October 2019). Based on the evolution of equatorial zonal winds in those CMIP6 models (Rao et al. 2020), 11 CMIP6 models can reproduce QBO-like cycles in the tropical stratosphere. Most of those 11 CMIP6 models that have a QBO are high-top models with a model top at or above the 1-hPa pressure level or higher than ~50 km, except that BCC-CSM2-MR has a relatively lower model top. The horizontal resolution in CMIP6 models is generally higher than in CMIP5 models, although a finer horizontal resolution appears less important than a finer vertical resolution to simulate the QBO. The first historical experiment is available for nearly all CMIP5/6 models in Table 1. The affiliation, nationality, horizontal resolution, model top and levels, and reference for each CMIP5/6 model are listed in Table 1.

b. Methods

Considering that the HT relationship was originally identified using zonal mean zonal wind anomalies at 50 or 30 hPa (Holton and Tan 1980; Baldwin et al. 2001; Garfinkel and Hartmann 2007), and that the QBO winds at 50 hPa and below are largely underestimated in models (Rao et al. 2020), the QBO index is defined as the zonal mean zonal wind anomalies at 30 hPa (QBO30) over the equator (5°S–5°N). The HT relationship can be clearly observed and modeled if a threshold of $\pm 5 \text{ m s}^{-1}$ for equatorial zonal winds is used to select westerly and easterly QBO winters for the Northern Hemisphere (Rao et al. 2020), but the tropospheric anomalies are smaller and even nearly undetectable with this threshold for some models. Instead, we use a larger threshold of $\pm 7.5 \text{ m s}^{-1}$ to define the QBO westerly and easterly phases (WQBO and EQBO) in this paper to better detect the tropospheric pathways. The relatively large threshold in this study can guarantee a consistent QBO sign at 30 hPa and lower stratosphere in the tropics. With a uniform criterion for the reanalysis and models, the WQBO winter is selected if the winter-mean (December–February) QBO30 exceeds 7.5 m s^{-1} , and the EQBO winter is selected if the winter-mean QBO30 falls below -7.5 m s^{-1} . We also assessed sensitivity by using a larger threshold

TABLE 2. Westerly QBO ($QBO_{30} \geq 7.5 \text{ m s}^{-1}$) and easterly QBO ($QBO_{30} \leq -7.5 \text{ m s}^{-1}$) winter (December–February) sizes and their ratio in the reanalysis and CMIP5/6 models. The timespan is 1958–2014 for the reanalysis, 1850–2005 for CMIP5 models, and 1850–2014 for CMIP6 models. Note that the QBO threshold is ± 7.5 to get a more robust and detectable tropospheric response. The ± 5 threshold is used in Rao et al. (2020) to study the Holton–Tan (HT) relationship. The composite Niño-3.4 difference between EQBO and WQBO is also shown in the last column to explore any possible relationship between QBO and ENSO. The composite Niño-3.4 is based on the original anomaly data without the ENSO signal removed.

| Model or baseline | EQBO | WQBO | Ratio | Composite Niño-3.4 |
|-------------------|------|------|-------|--------------------|
| JRA-55 | 21 | 19 | 1.11 | −0.01 |
| CESM1-WACCM | 42 | 57 | 0.74 | 0.01 |
| CMCC-CMS | 12 | 20 | 0.60 | 0.42 |
| HadGEM2-CCS | 53 | 60 | 0.88 | −0.10 |
| MIROC-ESM-CHEM | 48 | 62 | 0.77 | −0.02 |
| MIROC-ESM | 61 | 68 | 0.90 | −0.02 |
| MPI-ESM-MR | 63 | 65 | 0.97 | 0.04 |
| BCC-CSM2-MR | 28 | 23 | 1.22 | 0.02 |
| CESM2-WACCM | 36 | 26 | 1.38 | −0.58 |
| CNRM-CM6.1 | 39 | 47 | 0.83 | −0.07 |
| CNRM-ESM2.1 | 43 | 47 | 0.91 | −0.05 |
| EC-Earth3 | 53 | 61 | 0.87 | −0.03 |
| EC-Earth3-Veg | 50 | 54 | 0.93 | 0.11 |
| HadGEM3-GC31-LL | 61 | 70 | 0.87 | −0.55 |
| IPSL-CM6A-LR | 54 | 64 | 0.84 | −0.17 |
| MIROC6 | 45 | 46 | 0.98 | −0.19 |
| MRI-ESM2.0 | 62 | 70 | 0.89 | 0.01 |
| UKESM1.0-LL | 65 | 77 | 0.84 | 0.14 |

(e.g., $\pm 10 \text{ m s}^{-1}$) for each model, but the composite pattern is nearly unchanged. The WQBO and EQBO winter sizes for the JRA-55 reanalysis (Kobayashi et al. 2015) and CMIP5/6 models are listed in Table 2.

To better understand the North Pacific response to the QBO, the contribution of the downward arching zonal winds to the formation of local relative vorticity anomalies is also analyzed (i.e., $\zeta = -\partial u/\partial y$). With the quasigeostrophic assumption, the development of low relative vorticity anomalies should be balanced by a geopotential height anomaly center (i.e., $\zeta \sim -z$). Some previous studies emphasized that the impacts of QBO might be entangled with ENSO (e.g., Garfinkel and Hartmann 2007; Domeisen et al. 2019; Rao et al. 2019). All the composite response graphics are calculated as a difference between EQBO and WQBO after the ENSO signal is removed from each dataset using a regression method, and their significance level is estimated with the Student's t test. To remove the ENSO signal, the product of the regression coefficient against the winter-mean Niño-3.4 index and the winter-mean Niño-3.4 index is subtracted from the anomaly field for a variable of interest (Rao and Ren 2020). Unless specified, all composites are based on the anomaly field with the ENSO signal removed for each dataset, although a possible nonlinear impact of ENSO and QBO might not be removed by this method. In the tropics, we also use the outgoing longwave radiation (OLR) and rainfall to denote convection: stronger deep convection is associated with clouds at higher altitudes and therefore lower OLR, and hence we expect heavier precipitation associated with lower OLR. Because the Eliassen–Palm flux (F_y, F_z) and its divergence, as well as the residual streamfunction and residual vertical velocity (\bar{v}^*, \bar{w}^*), in the transformed Eulerian-

mean frame have been reported in Rao et al. (2020) to evaluate the HT mechanism and the direct meridional circulation cell response, we will put more focus on the tropospheric pathways in this study.

3. Stratospheric polar vortex pathway for the QBO's impact on the troposphere

The composite zonal-mean zonal wind difference in December–February between EQBO and WQBO is shown in Fig. 1 for the reanalysis and models. Because the QBO zonal winds in the tropical stratosphere marked by a gray box are much larger than in the extratropics, the contour intervals inside the box and outside are different (5 and 0.5 m s^{-1} , respectively). Compared with WQBO, easterly anomalies develop in the circumpolar stratosphere with a maximum center at 65°N during EQBO, which extend downward into the troposphere and near surface in JRA-55 (Fig. 1a). This is a typical pattern of negative NAM in the extratropics, with the polar height/pressure rising and midlatitude height/pressure decreasing, which corresponds to a deceleration of the stratospheric polar jet. In the tropics, the westerlies above the QBO easterlies centered at 30 hPa tend to arch downward, indicated by a patch of westerlies between 30° and 40°N . Such a downward arching of the equatorial zonal winds is usually accompanied by the meridional circulation cell of the QBO (Haigh et al. 2005; Garfinkel and Hartmann 2011a,b; Rao et al. 2020).

The negative NAM response to EQBO (i.e., the HT effect) is simulated by most models, but the easterly anomalies in the stratospheric circumpolar region are underestimated in the models (Figs. 1b–r). The QBO winds are nudged in CESM1-WACCM, and the composite easterlies in the equatorial

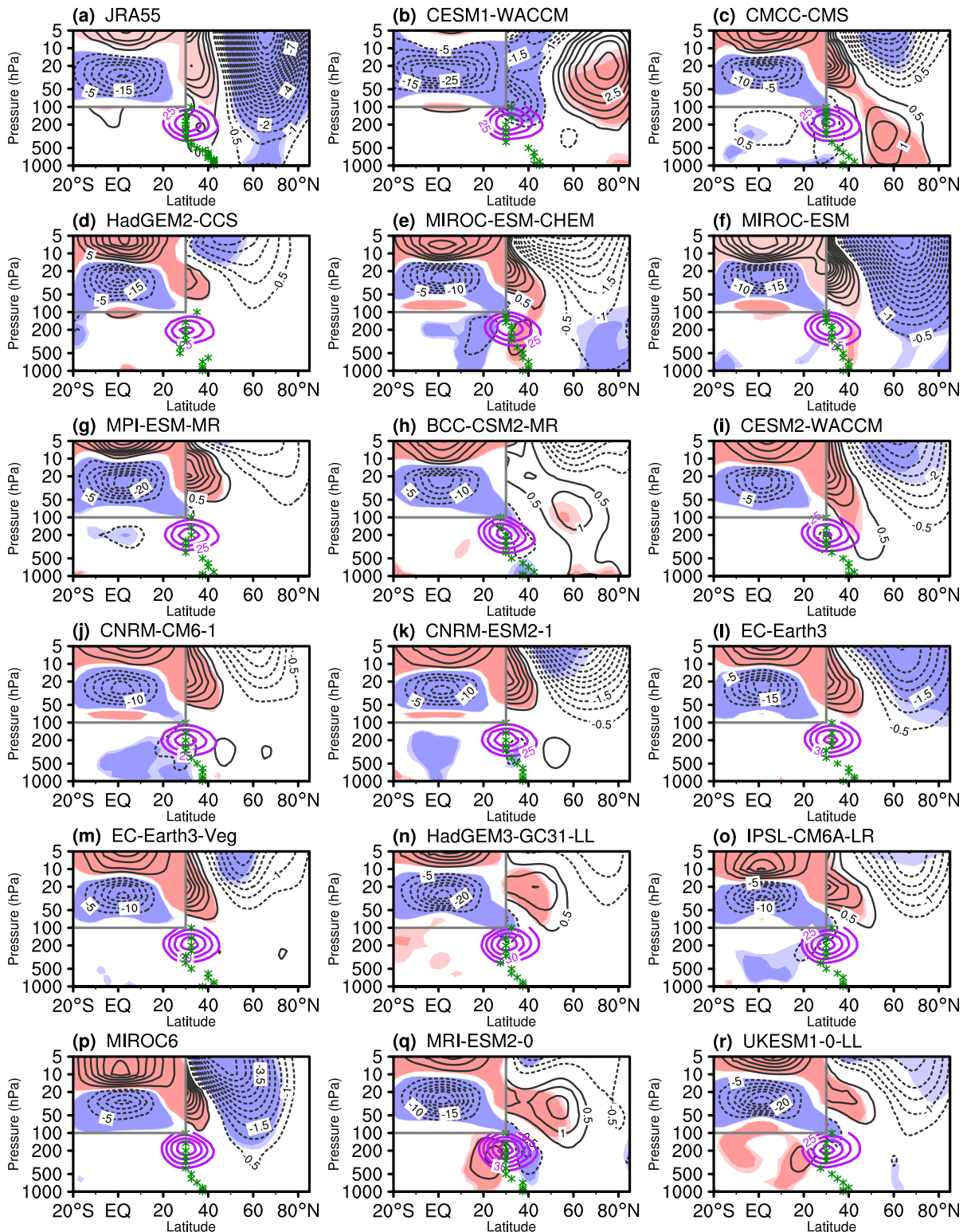


FIG. 1. Pressure–latitude cross sections of zonal-mean zonal wind differences (contours; m s^{-1}) between EQBO and WQBO with the ENSO signal removed from 1000 to 5 hPa in the northern winter (December–February) for (a) the JRA-55 reanalysis, (c)–(h) 6 CMIP5 models, and (i)–(r) 11 CMIP6 models. The equatorial stratospheric QBO winds encircled by the gray box are nearly an order larger than outside, so the contour interval is 5 (0.5) m s^{-1} inside (outside) the gray box to clearly display the winds. The zero contours are skipped for clarity. The light (dark) shadings mark the wind anomalies at the 90% (95%) confidence level according to Student's t test. The purple contours are the climatological zonal mean zonal winds for the subtropical tropospheric jet (starting from 25 m s^{-1} with a contour interval of 5 m s^{-1}). The green asterisk marks the subtropical jet center from 1000 to 100 hPa.

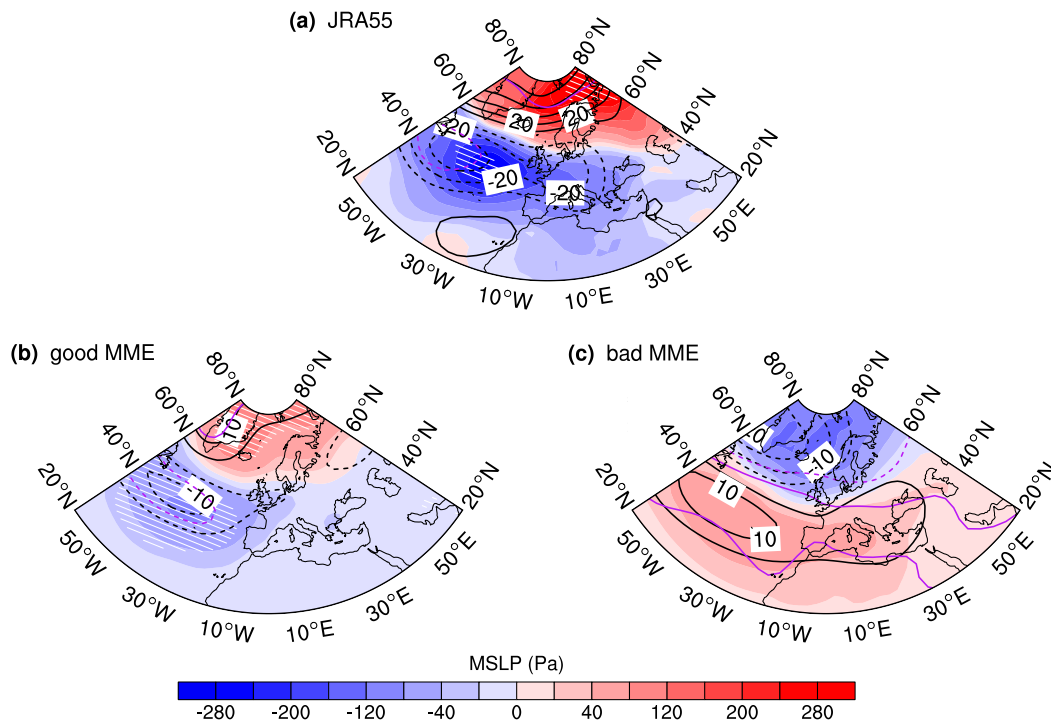


FIG. 2. Composite differences in the mean sea level pressure (MSLP; shading; Pa) and 200-hPa geopotential height (contours; gpm) between EQBO and WQBO with the ENSO signal removed in the northern winter (December–February) for (a) JRA-55, (b) the ensemble mean of 7 models with a realistic HT relationship shown in Figs. 1e,f,i,k,l,p,r and (c) the ensemble means of the remaining 10 models. Hatched regions and purple contours mark the MSLP and 200-hPa geopotential height anomalies at the 95% confidence level according to Student's t test, respectively.

stratosphere extend farther north than in the other models (Fig. 1b). The downward arching of zonal-mean easterlies from the tropical stratosphere in CESM1-WACCM also extend unrealistically far northward. The circumpolar easterly response in this model is situated much higher, and the lower stratospheric easterlies over the Arctic in the reanalysis are replaced by weak westerlies. In contrast, the HT relationship and the tropospheric negative AO response is better simulated by MIROC-ESM-CHEM, MIROC-ESM, CESM2-WACCM, CNRM-ESM2.1, EC-Earth3, MIROC6, and UKESM1.0-LL (Figs. 1e,f,i,k,l,p,r).

The stratospheric polar vortex pathway mainly dominates the Arctic region and the North Atlantic Ocean–Europe sector via the AO/NAO response. The tropospheric response in the Atlantic–European region to the QBO is shown in Fig. 2 for models with (i.e., the circumpolar easterly anomalies extend downward to the troposphere) or without (i.e., the circumpolar easterly anomalies fail to extend downward to the troposphere) a realistic HT relationship. Most models can capture the stratospheric polar vortex response to QBO, but many models still fail to simulate a QBO–AO/NAO relationship due to the modeling bias associated with the underestimated polar vortex response. A strong negative (positive) NAO-like response is observed during EQBO (WQBO) winters in JRA-55 (Fig. 2a; also see Fig. 7 in Gray et al. 2018), while both lobes of the NAO (i.e., the low center in the midlatitude Atlantic and the high

center in high latitudes) during EQBO are somewhat underestimated even in the ensemble mean of good models (Fig. 2b). In the ensemble mean of models without a decent HT relationship, the response is of the wrong sign (Fig. 2c). Such a bias might limit our application of the HT mechanism to prediction of the European and Arctic climate with most models.

The unrealistic AO/NAO response to the QBO in the models that fail to capture the HT effect is likely related to the probability distribution of the eight QBO phases in the wintertime months (Rao et al. 2020). The HT relationship is strongest during QBO phase 3 (7) when the 30-hPa westerlies (easterlies) over the equator begin to decrease, and the lower stratospheric westerlies (easterlies) are maximized (Gray et al. 2018; Andrews et al. 2019; Rao et al. 2020). Figure 3 shows the relationship between the NAO/AO-like response magnitude in December–February and the total probability density function (PDF) of the QBO phases 3 and 7 in late autumn–early winter. All models and MME simulate a lower PDF of QBO phases 3 and 7 than the reanalysis, and the inter-dataset correlation (0.44) between the total PDF and the polar cap mean sea level pressure (MSLP) response to the QBO with the ENSO signal removed reaches the 90% confidence level ($\alpha \leq 0.1$). The composite between QBO phases 7 and 3 is stronger than the EQBO minus WQBO composite difference especially for the good MME in CMIP5/6 models (Fig. S2 in the online supplemental material).

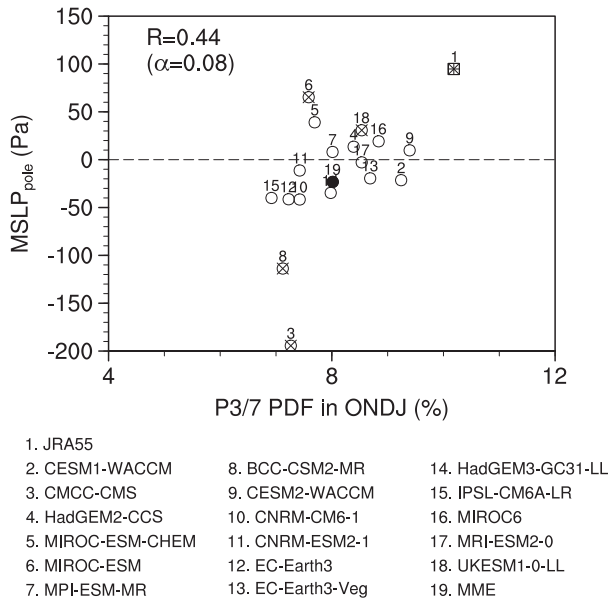


FIG. 3. Relationship between the mean sea level pressure (MSLP) response to QBO in the polar cap region (60° – 90° N; ordinate; Pa) with the ENSO signal removed during the northern winter (December–February) and the total probability density function (PDF) for the QBO phases 3 and 7 in late autumn–early winter (October–January). The QBO phase 7 (3) happens when the 30-hPa easterlies (westerlies) weaken but the lower stratospheric easterlies (westerlies) grow. The correlation between the total PDF and the polar cap MSLP response (R) and its significance level (α) for the reanalysis and models (datasets 1–18) are shown on the top left. The number above the scattered point marks the data source. The circle (square) is shown for models (JRA-55). The cross sign denotes the composite MSLP response at the 95% confidence level, and the plus sign means the total PDF in October–January $> 10\%$ (only the observation shows this, see No. 1). The PDF of QBO phases in models is relatively much more uniform ($100\%/12$ months/8 phases $\approx 1.04\%$ month $^{-1}$ phase $^{-1}$; for phases 3 and 7 in October–January, the total PDF = 1.04% month $^{-1}$ phase $^{-1} \times 2$ phases $\times 4$ months = 8%). The estimated value (8%) is especially true for the multimodel ensemble mean (MME; see No. 19), while the observation shows a much higher PDF for QBO phases 3 and 7 in October–January (see No. 1).

4. North Pacific pathway for the QBO's impact on the troposphere through downward arching winds

Based on the zonal mean response pattern in Fig. 1, the downward arching of the equatorial zonal wind to the tropical and subtropical troposphere is simulated to different degrees of success. The easterly anomalies fail to arch downward from the tropical stratospheric at 50 hPa to the upper troposphere, whereas the arching of westerlies from the upper stratosphere might explain the midlatitude westerly anomalies (Fig. 1a). Some models simulate this feature more strongly than is evident in reanalysis data (Figs. 1e,f). Other models can well simulate the horseshoe shape of QBO winds in lower latitudes, but their central latitudes are incorrectly positioned. For example, the tropospheric midlatitude westerlies extend farther

poleward in CMCC-CMS, BCC-CSM2-MR, CESM2-WACCM, HadGEM3-GC31-LL, IPSL-CM6A-LR, MRI-ESM2.0, and UKESM1.0-LL (Figs. 1c,h,i,n,o,q,r).

The downward arching of the QBO winds into the subtropical troposphere is most prominent in the Pacific sector, likely due to the more equatorward location of the eddies and jet in this sector (Garfinkel and Hartmann 2011a,b). The pressure–latitude cross sections of difference in zonal winds averaged over the Pacific sector between EQBO and WQBO are shown in Fig. 4. Compared with the zonal-mean response in the tropics and NH extratropics, the observed response in the Pacific sector is stronger (Fig. 4a), consistent with Garfinkel and Hartmann (2011a,b). The equatorial QBO easterlies centered at 30 hPa and westerlies aloft tend to arch downward anomalies in the Pacific sector (cf. Figs. 1a and 4a). By focusing on the Pacific sector, and based on the reanalysis, it is also shown that seven models can simulate the tropospheric easterly anomaly center from 20° to 40° N, including HadGEM2-CCS, MPI-ESM-MR, CESM2-WACCM, CNRM-CM6.1, EC-Earth3-Veg, HadGEM3-GC3.1-LL, and MIROC6 (Figs. 4d,g,i,j,m,n,p). In contrast, the tropical tropospheric westerlies anomalies associated with the descending momentum of the QBO observed in the Pacific sector are present in fewer models (Figs. 4d,j,m,n,p,r).

To better understand the importance of the downward arching QBO momentum for the North Pacific circulation, the composite differences in the 200-hPa height anomalies during mid-to-late winter between EQBO and WQBO are shown in Fig. 5. The reanalysis reveals that a high anomaly center forms over the North Pacific in late winter during EQBO (Fig. 5a), which is only reproduced in models with a successful easterly downward arching into the troposphere over the Pacific sector (Fig. 5b). In contrast, the high center over North Pacific is not simulated in other models with a QBO wind arching incorrectly in its position and/or width (Fig. 5c).

To test the relationship between the QBO easterlies averaged over 20° – 40° N in the Pacific sector and the North Pacific circulation, a model-by-model scatterplot of the downward-arching QBO wind anomalies in the Pacific versus the North Pacific height response is shown in Fig. 6. The zonal wind anomalies over 20° – 40° N, 160° – 220° E at 200 hPa are negatively correlated with the North Pacific height response with a correlation of -0.71 after the ENSO signal is removed (Fig. 6a). For most models and the reanalysis, the height response over the North Pacific to the QBO is mainly explained by the direct downward-arching of the equatorial stratospheric winds. Specifically, the arching easterlies during EQBO correspond to a high height response in the reanalysis and some models (e.g., HadGEM2-CCS, CNRM-CM6.1, and HadGEM3-GC31-LL in the second quadrant) and the unrealistic westerlies in some models are consistent with their low height response over the North Pacific (e.g., CMCC-CMS and MRI-ESM2.0 in the fourth quadrant).

The subtropical zonal wind anomalies induced by the QBO-induced mean meridional circulation modify the background circulation by changing the vorticity over the North Pacific and hence the geopotential height. The negative relationship between the meridional wind shear anomalies

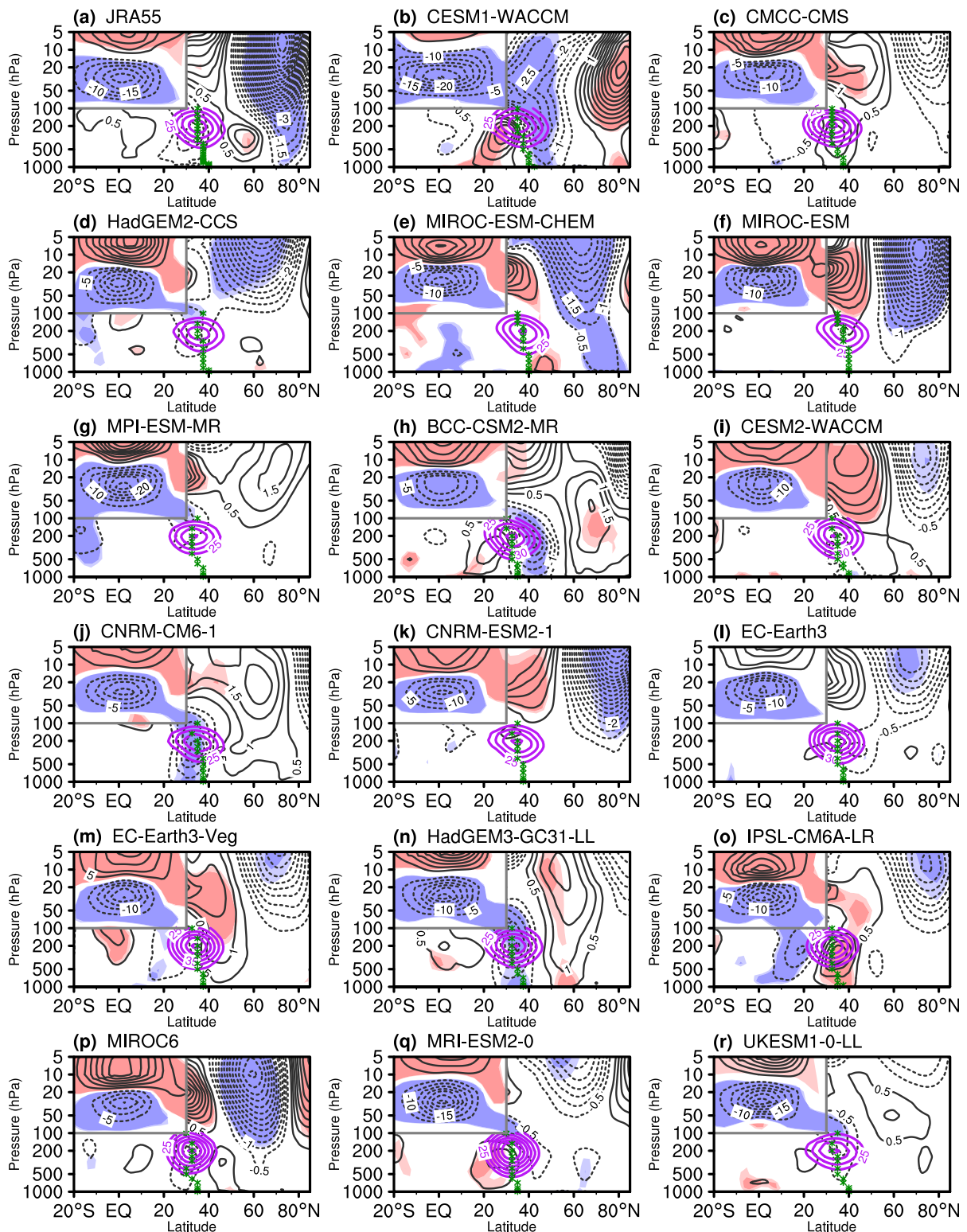


FIG. 4. As in Fig. 1, but for the pressure–latitude cross sections of zonal-mean zonal winds (contours; m s^{-1}) in the Pacific sector (160° – 220°E) from 1000 to 5 hPa during mid-to-late winter (January–March). The purple contours are the climatological zonal mean zonal winds for the subtropical tropospheric jet in the Pacific sector (starting from 25 m s^{-1} with a contour interval of 5 m s^{-1}). The green asterisk marks the subtropical jet center in the Pacific center from 1000 to 100 hPa.

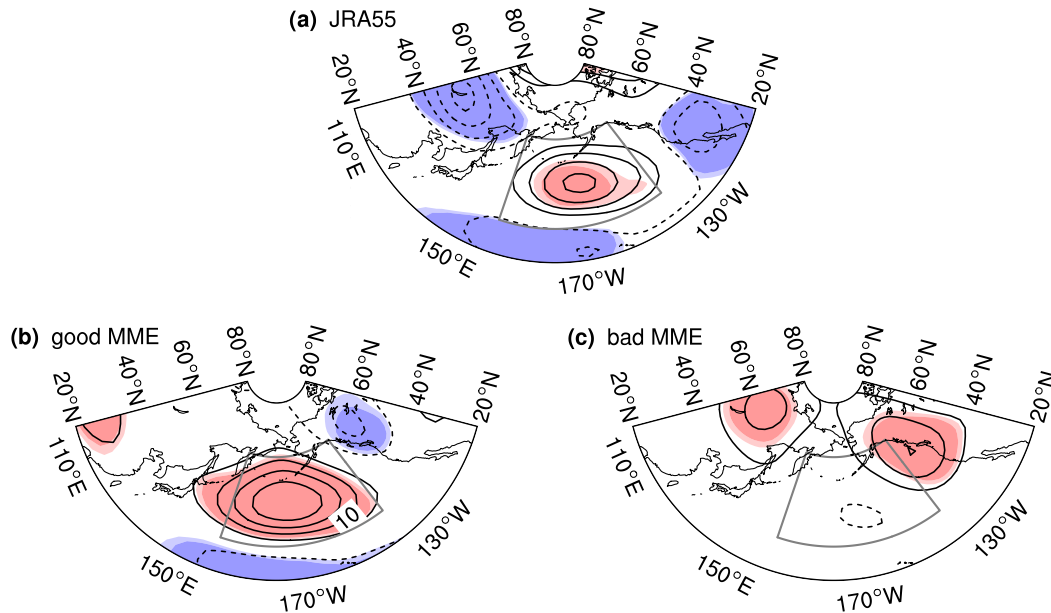


FIG. 5. Composite differences in the 200-hPa geopotential height anomalies (contours; gpm) between EQBO and WQBO with the ENSO signal removed in the northern mid-to-late winter (January–March) for (a) JRA-55, (b) the ensemble mean of 7 models with a successful simulation of the QBO wind arching in Figs. 4d, 4g, 4i, 4j, 4m, 4n, and 4p, and (c) the ensemble means of the remaining 10 models. The zero contours are skipped for clarity. Light (dark) shadings mark the height anomalies at the 90% (95%) confidence level according to Student's t test. The gray box (30° – 60° N, 160° – 220° E) denotes the observed North Pacific height response center.

and the North Pacific height (Fig. 6b) becomes even stronger than that in Fig. 6a. Namely, the downward arching QBO winds can excite an anomalous vorticity, thereby the height field adjusts to reach a new quasigeostrophic balance. Models without anticyclonic vorticity in the Pacific sector fail to simulate a high center over North Pacific (e.g., CMCC-CMS, MIROC-ESM, MRI-ESM2.0). It is also noticed that CESM1-WACCM and BCC-CSM2-MR also reproduce a North Pacific high center, but farther poleward than the reanalysis, although the meridional wind shear between 40° – 60° N and 20° – 40° N is cyclonic (the first quadrant in Fig. 6b). CESM1-WACCM also simulates a much wider QBO in the tropical stratosphere as compared to any other model or to the reanalysis (Figs. 1b and 4b), consistent with the northward shift of the North Pacific high. This mechanism is more applicable to North Pacific where the downward impact of the stratospheric polar vortex variations is relatively weak compared with that in North Atlantic.

Finally, there is some indication in reanalysis that winds in the equatorial upper troposphere are of opposite sign to that in the lower stratosphere; for example, the equatorial troposphere is dominated by weak westerly anomalies during EQBO phases (Fig. 1a). However, the weak westerlies are evident only in CESM1-WACCM, HadGEM2-CCS, and UKESM1.0-LL (Figs. 1b,d,r), with most models failing to simulate this feature (although in some the opposite-signed response is evident in the tropopause transition layer).

5. Tropical convection pathway over the Maritime Continent for the QBO's impact on the troposphere

a. Tropical deep convection response as estimated by OLR and rainfall

Previous studies also emphasize the direct influence of the QBO on tropical deep convection (Collimore et al. 2003; Garfinkel and Hartmann 2011b; Liess and Geller 2012; Nie and Sobel 2015; Gray et al. 2018), which can excite Rossby wave trains and related teleconnections spanning the tropics and extratropics. Enhanced deep convection in the tropics usually corresponds to more latent heat release into the troposphere and warm temperature anomalies there (Rao and Ren 2016, 2018; Kim et al. 2018).

Figure 7 shows the composite difference in the OLR between EQBO and WQBO from JRA-55 and models, with lower OLR corresponding to more high clouds and generally more convection. The convection response is observed to be zonally asymmetric at the equator: convection over the eastern Indian Ocean–Maritime Continent–western Pacific Ocean region (15° S– 15° N, 60° – 160° E; the purple box in Fig. 7) is largely intensified, but the convection in other tropical regions is more unorganized and weaker (Fig. 7a), consistent with Collimore et al. (2003) and Garfinkel and Hartmann (2011a). Not all models can reproduce the local enhanced convection: Seven of the evaluated models can simulate the negative OLR anomalies near the Maritime Continent (Figs. 7b,d–h,o), despite an underestimation in two models (Figs. 7d,o). The OLR anomalies

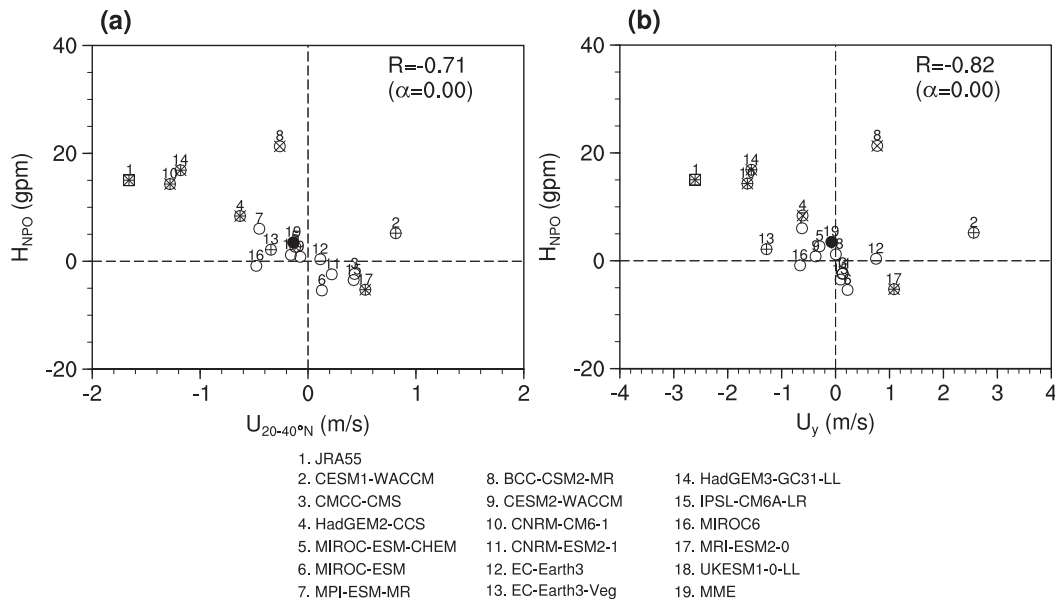


FIG. 6. (a) Relationship between the downward-arched QBO wind anomalies in the Pacific and the North Pacific height response in CMIP5/6 in the northern winter (December–February). The composite wind differences are averaged over the midlatitude Pacific (20° – 40° N, 160° – 220° E) at 200 hPa with the ENSO signal removed for every model, while the composite height differences are averaged over the North Pacific (30° – 60° N, 160° – 220° E; the box in Fig. 5) with the ENSO signal removed. The correlation between the midlatitude Pacific zonal winds and the North Pacific height (R) and its significance level (α) are shown on the top right. The number above the scattered point marks the data source. The circle (square) is shown for models (JRA-55), and the cross (plus) sign denotes the composite value of the y axis (x axis) at the 95% confidence level. (b) As in (a), but for the relationship between the meridional wind shear ($-\partial u/\partial y$) anomalies in the Pacific and the North Pacific height response in CMIP5/6 with the ENSO signal removed. The meridional wind shears at 200 hPa are represented by the zonal wind difference between two latitude bands in the Pacific sector (south band: 20° – 40° N, 160° – 220° E; north band: 40° – 60° N, 160° – 220° E). The correlation between the meridional wind shear and North Pacific height (excluding the outliers, CESM1-WACCM and BCC-CSM2-MR) and its significance are shown on the top right.

outside the purple box are different in most models. HadGEM3-GC31-LL, MRI-ESM2.0, and UKESM1.0-LL also simulate an intensified convection center, but it is shifted farther eastward to the date line (Figs. 7n,q,r). Convection over the Maritime Continent in those three models is opposite in sign to the reanalysis.

To test the self-consistency of each dataset, the tropical precipitation response to the QBO during the northern winter is also shown in Fig. 8. The pattern of the tropical rainfall in Fig. 8 is highly consistent with the OLR in Fig. 7. Specifically, anomalously enhanced rainfall is present in most parts of the eastern Indian Ocean–Maritime Continent–western Pacific Ocean region due to local enhanced moist convection (Fig. 8a), and rainfall anomalies outside the purple box are much more scattered and insignificant. Some models simulate positive precipitation anomalies near the Maritime Continent (Figs. 8b,d–h,m,o), similar to the reanalysis; in contrast, the anomalies in four models are fairly weak (Figs. 8e,f,m,o). Consistent with the negative OLR anomalies, the positive rainfall anomalies in CMCC-CMS, MRI-ESM2.0, and UKESM1.0-LL also shift toward the date line; the rainfall near the Maritime Continent is anomalously reduced (Figs. 8c,q,r).

The deep convection response might be associated with changes in the buoyancy frequency in the lower stratosphere and upper troposphere (atmospheric stability). To further

confirm this, the buoyancy frequency squared (N^2) differences between EQBO and WQBO near the tropopause at 100 hPa are shown in Fig. 9. It is shown once again that the tropical near-tropopause static stability decreases (i.e., negative N^2 difference) over the Maritime Continent in the reanalysis (Fig. 9a), which may be expected to enhance deep convection locally. In the tropical middle and eastern Pacific, the buoyancy frequency squared is also decreased but with a narrower latitude band (Fig. 9a). More than half of the models simulate the observed negative N^2 anomalies over the Maritime Continent (Figs. 9b,d,f,g,i,l–r). In contrast, the negative N^2 anomalies in the focused region (see the green box) are much smaller in BCC-CSM2-MR, CESM2-WACCM, and CNRM-ESM2.1 (Figs. 9h,i,k), and the anomaly sign is unrealistic in CMCC-CMS, MIROC-ESM-CHEM, and CNRM-CM6.1 (Figs. 9c,e,j). The decrease in the N^2 anomalies is also simulated over eastern Pacific in most models (Figs. 9b,d,g–i,l–r). Considering that the composite N^2 difference between EQBO and WQBO using the QBO30 index might not be maximized, the composite N^2 difference between the QBO phases 7 and 3 is provided in Fig. S3. The N^2 patterns for most models are qualitatively similar for both composites (Fig. 9 and Fig. S3).

In summary, compared with the consistent and robust circulation anomalies in the tropical stratosphere in all datasets as

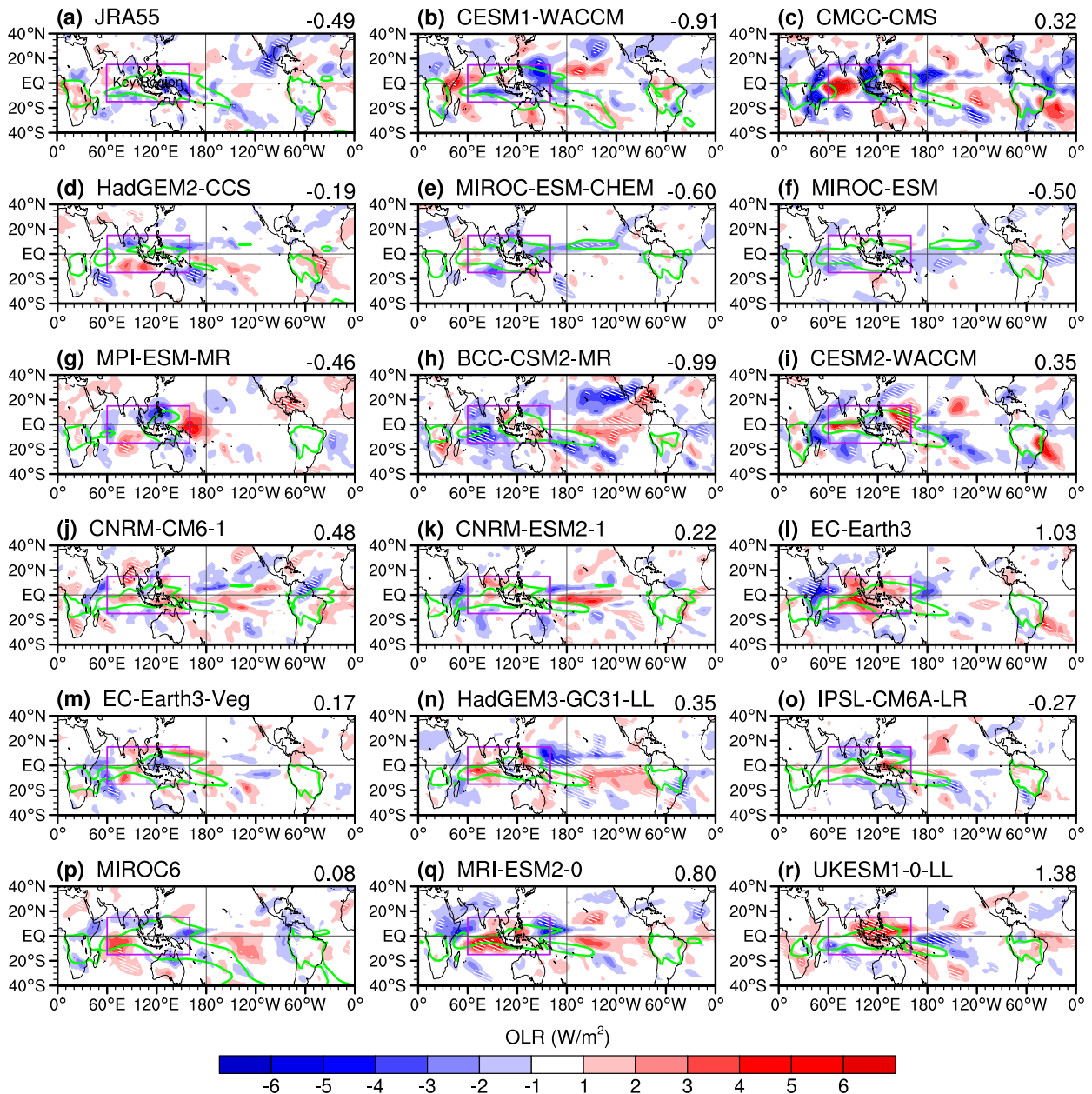


FIG. 7. Composite differences in the outgoing longwave radiation (OLR; shading; W m^{-2}) between EQBO and WQBO with the ENSO signal removed in the northern winter (December–February) for (a) the JRA-55 reanalysis, (c)–(h) 6 CMIP5 models, and (i)–(r) 11 CMIP6 models. The purple box (15°S – 15°N , 60° – 160°E) marks the key Indo-Pacific region, where enhanced convection is detected in the observation. The area-weighted composite OLR difference in the purple box is printed on the top right for each plot. The white hatched regions mark the OLR anomalies at the 90% confidence level. The green contours ($=230 \text{ W m}^{-2}$) mark the climatological lowest OLR centers (i.e., the strongest convection centers) in the tropics.

shown in Figs. 1 and 4, most models also simulate an enhanced but insignificant convection anomaly over the Maritime Continent during EQBO. No significant convection anomalies over the eastern Pacific are observed in the reanalysis and in most models, either. The enhanced deep convection (although insignificant for some datasets) during EQBO can only be detected over the Indo-Pacific Ocean in the reanalysis and

most models, while the convection response outside the Maritime Continent is relatively weak and not salient.

b. Little contribution from the QBO-related convection to the North Pacific high response

Tropical convection creates a divergent flow in the upper troposphere, which acts as a wave source for a teleconnection

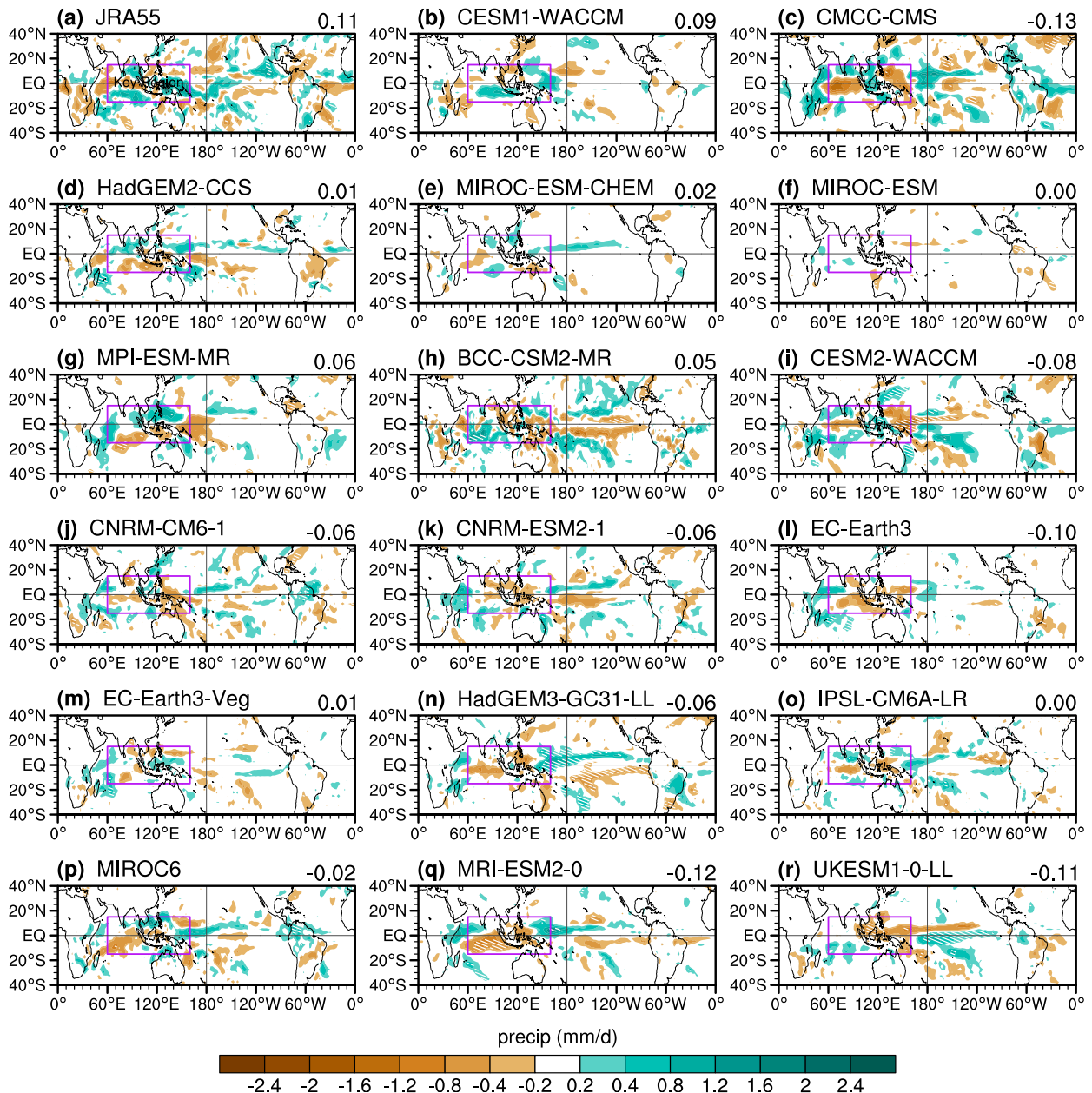


FIG. 8. As in Fig. 7, but for composite differences in the precipitation (shading; mm day^{-1}) between EQBO and WQBO with the ENSO signal removed in the northern winter for (a) the JRA-55 reanalysis, (c)–(h) 6 CMIP5 models, and (i)–(r) 11 CMIP6 models.

from the tropics to high latitudes (Liess and Geller 2012; Gray et al. 2018). Convective heating over the tropical Indian Ocean can also excite a high center over North Pacific, which is opposite to the impact (i.e., a low center over North Pacific) of the tropical Pacific forcing (Fletcher and Kushner 2011; Rao and Ren 2016). Is the observed North Pacific high response mainly caused by the enhanced convection over Maritime Continent, or by the direct downward-arching zonal winds of the QBO winds?

We examine four pairs of parameters to confirm the consistency of the tropical convection response with OLR, precipitation, vertical velocity, and near-tropopause buoyancy

frequency over the Indo-Pacific Ocean in Fig. 10. A negative correlation between OLR and the precipitation over the Indo-Pacific Ocean is established from their model-by-model scatterplot (Fig. 10a). The observed negative OLR anomalies are successfully simulated in seven models (the second quadrant), while other models reproduce positive OLR and less rainfall (the fourth quadrant). The positive rainfall anomalies can also be manifested by the enhanced upwelling for some models (models 2, 4–8, 13, and 15; the first and second quadrants in Fig. 10b). The enhanced convection and upwelling over the Indo-Pacific Ocean is associated with a reduction in

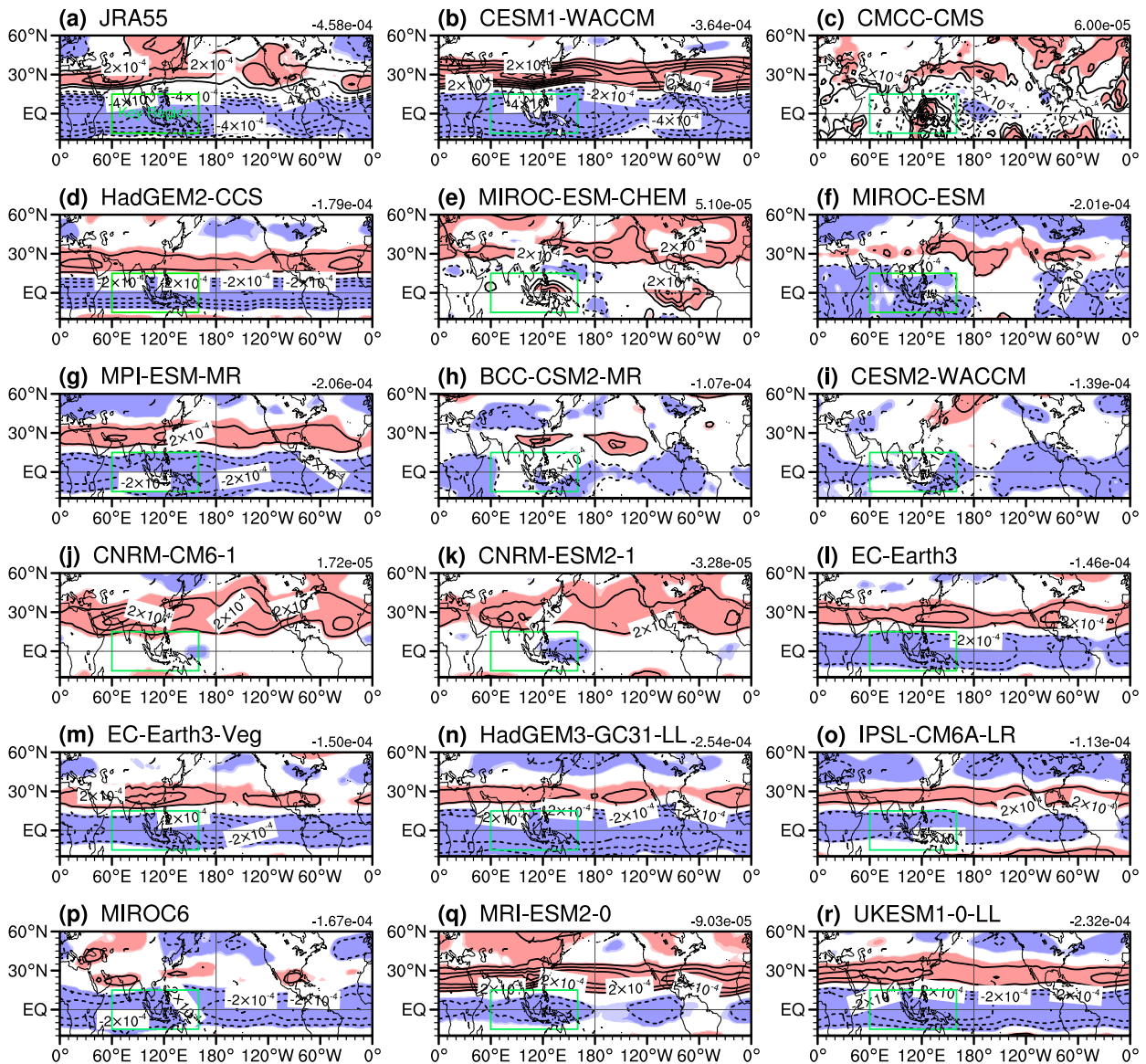


FIG. 9. Composite differences in the buoyancy frequency squared (N^2) at 100 hPa (contours; s^{-2}) between EQBO and WQBO with the ENSO signal removed in the northern winter (December–February) for (a) the JRA55 reanalysis, (c)–(h) 6 CMIP5 models, and (i)–(r) 11 CMIP6 models. The green box (15°S – 15°N , 60° – 160°E) is identical to Figs. 7 and 8, marking the key convection region. The area-weighted composite N^2 difference in the purple box is printed on the top right for each plot. Light (dark) shadings mark buoyancy frequency squared anomalies at the 90% (95%) confidence level.

near-tropopause N^2 in the reanalysis and some models (the third quadrant in Fig. 10c): after the ENSO variability is removed, the correlation between the local vertical velocity and 100-hPa buoyancy frequency among multiple models is 0.44 with a 90% confidence level ($\alpha \leq 0.1$). Therefore, the convection response might be a key chain linking the QBO forcing in the tropical stratosphere and the local climate anomalies in Indo-Pacific region.

Next, we compare the tropical convection–North Pacific response chain and the downward arching QBO winds–North Pacific response relationship (Fig. 10d vs Fig. 6). The North Pacific height response at 200 hPa tends to be negatively

correlated with the OLR anomalies over Indo-Pacific Ocean in models at a low confidence level ($\alpha = 0.30$): there is not a robust relationship between enhanced convection (i.e., negative OLR anomalies) over the Indo-Pacific Ocean and the high center over North Pacific in models. Namely, the contribution by the tropical convection-excited teleconnection to the North Pacific circulation is much weaker than that directly by the downward arching QBO winds. That is, the distribution of model coordinates in Fig. 10d is much more scattered than in Fig. 6, and the correlation amplitude also much smaller (-0.26 vs -0.71 – -0.82). Therefore, the North Pacific high response to EQBO is better explained by the QBO winds than the tropical

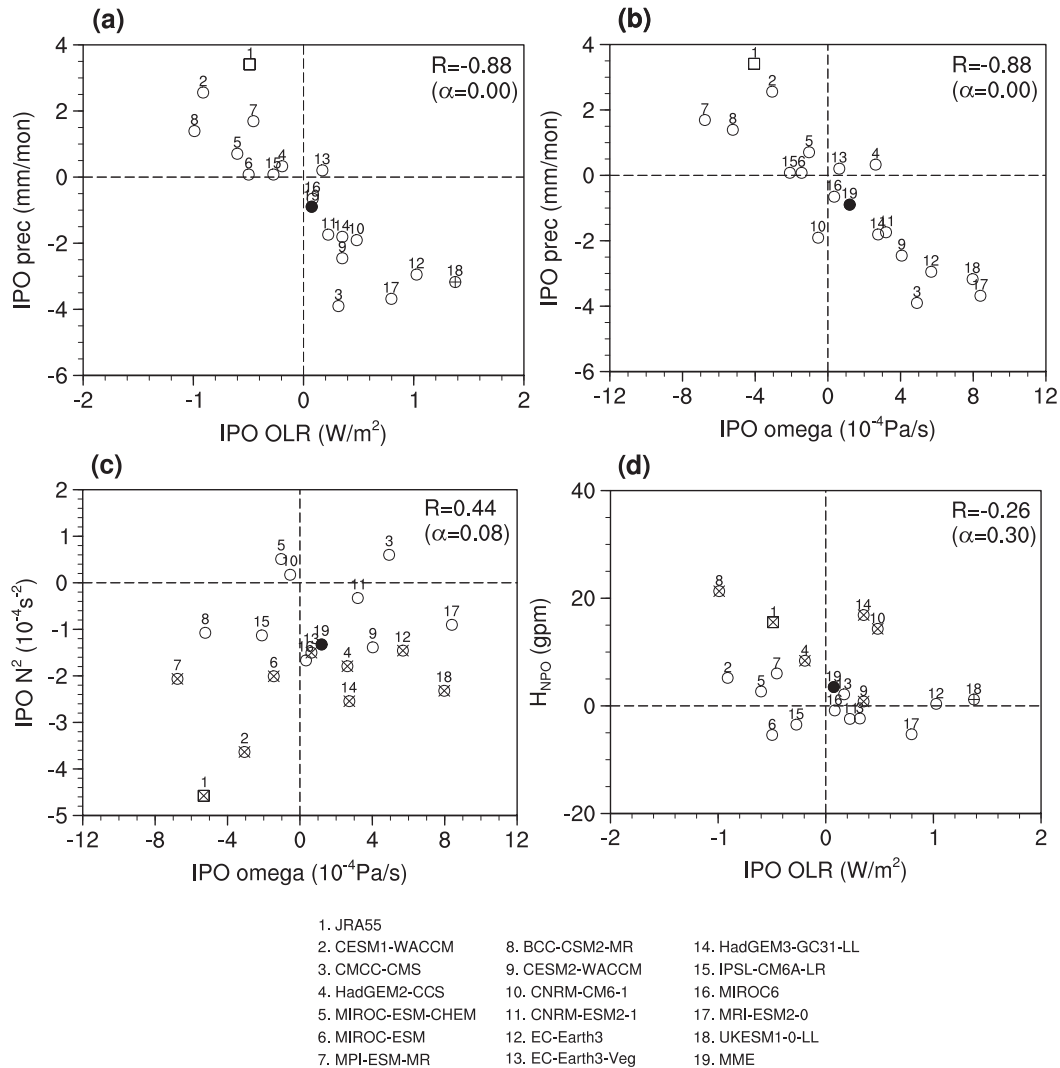


FIG. 10. (a) Scatterplot of the composite winter-mean (December–February) Indo-Pacific OLR difference between EQBO and WQBO vs the winter mean Indo-Pacific precipitation difference between EQBO and WQBO in the tropical key region (15°S – 15°N , 60° – 160°E) with the ENSO signal removed. (b) Scatterplot of the composite winter-mean (December–February) Indo-Pacific vertical velocity (averaged from 1000 to 100 hPa) difference between EQBO and WQBO vs the winter mean (December–February) Indo-Pacific precipitation difference between EQBO and WQBO in the tropical key region with the ENSO signal removed. (c) Scatterplot of the composite winter-mean (December–February) Indo-Pacific precipitation difference between EQBO and WQBO vs the 100-hPa buoyancy frequency squared (N^2) difference between EQBO and WQBO in the tropical key region with the ENSO signal removed. (d) Scatterplot of the composite winter-mean (December–February) Indo-Pacific OLR difference between EQBO and WQBO vs the mid-to-late winter (January–March) height difference between EQBO and WQBO at 200 hPa over the North Pacific (30° – 60°N , 160° – 220°E) with the ENSO signal removed. The circle (square) is shown for models (JRA-55), and cross (+) sign denotes the composite value of the y axis (x axis) at the 95% confidence level. The correlation between each pair of indicators (R) and its significance level (α) is also shown on the top right of each panel.

convection over the Indo-Pacific Ocean. On the other hand, the CMIP5/6 MME simulates an insignificant convection response over the Indo-Pacific Ocean (OLR, precipitation, omega, and near-tropopause buoyancy frequency square anomalies ≈ 0 ; Fig. 10), but they simulate downward arching QBO winds (Fig. 6).

6. Diverse connections between QBO and ENSO in CMIP5/6 models

Another concern we also try to address is the QBO–ENSO relationship in the reanalysis and CMIP5/6 models. It has been noticed that the running correlation between QBO and ENSO is unstable (e.g., Garfinkel and Hartmann 2007; Hu et al. 2012;

Domeisen et al. 2019). It is still not well understood whether the QBO–ENSO relationship in some decades may reflect a forced connection or is simply due to stochastic variability. Can we also extract any robust relationship between QBO and ENSO by using the reanalysis data? Is there any salient relationship between ENSO and QBO in observations when the data timespan becomes much longer?

Using the original anomaly data without the ENSO signal removed, the composite SST differences between EQBO and WQBO are shown in Fig. 11. No detectable SST anomalies appear in the tropical ocean basins, although significant SST anomalies form in the extratropics in JRA-55 (Fig. 11a). Therefore, no robust statistical relationship can be established between QBO and ENSO using the reanalysis data. Most models do not simulate significant SST anomalies in the tropical Pacific ENSO region (Figs. 11b,d–h,j–l,q), and no statistical relationship between QBO and ENSO is simulated in those models.

El Niño–like SST anomalies form in the tropical middle and eastern Pacific in CMCC-CMS, EC-Earth3-Veg, and UKESM1.0-LL (Figs. 11c,m,r), which is mainly driven by an anomalous anticlockwise Walker circulation cell over tropical Pacific (not shown) with anomalous upwelling/downwelling over the eastern/western Pacific Ocean. The downwelling and positive OLR anomalies over the Indo-Pacific Ocean in CMCC-CMS and UKESM1.0-LL are the strongest out of all datasets without the ENSO signal removed (not shown). The near-surface westerly anomalies of the anomalous anticlockwise Walker circulation cell in the western Pacific are a favorable and necessary condition for the initiation of an El Niño event. Some models show a QBO–ENSO relationship opposite to that in CMCC-CMS and UKESM1.0-LL (Figs. 11i,n–p): La Niña–like SST anomalies form in the tropical middle and eastern Pacific during EQBO in these models. CESM2-WACCM, HadGEM3-GC31-LL, IPSL-CM6A-LR, and MIROC6 have a much stronger downwelling branch over the middle and eastern Pacific, which corresponds to a strengthened clockwise Walker circulation. The near-surface easterly anomalies of the enhanced Walker circulation cell further accelerate the climatological trade winds and favor the development of a La Niña event (not shown).

To better understand the relationship between the Walker circulation and the eastern Pacific SSTs, scatterplots of the composite MSLP in the eastern Pacific and western Pacific (and their gradient) versus the Niño-3.4 index are shown in Fig. 12. Based on the multimodel correlation between MSLP and Niño-3.4 SST, the SST anomalies in the ENSO key region are more correlated with MSLP anomalies in the western Pacific than in the eastern Pacific (correlation amplitude: 0.71 vs -0.55). CMCC-CMS and UKESM1.0-LL (models 3 and 18 in Figs. 12a,b) are typical models with a negative QBO–ENSO relationship: a large positive MSLP anomaly in the western Pacific and/or negative MSLP anomaly in the eastern Pacific during EQBO correspond to an anomalous anticlockwise Walker circulation cell and induce westerly anomalies in the lower troposphere and sea surface, which are favorable for the initialization and development of warm SST anomalies in the ENSO key region (i.e., El Niño). On the contrary, CESM2-WACCM and HadGEM3-GC31-LL (models 9 and 14) are

typical models with a positive QBO–ENSO relationship: a large negative MSLP anomaly in the western Pacific and positive MSLP anomaly in the eastern Pacific during EQBO are modeled, indicating an acceleration of the climatological (clockwise) Walker circulation cell spanning across the Pacific. Most models simulate an insignificant MSLP response in the tropical Pacific, and the SST anomalies in the ENSO key region are also too weak to reach the ENSO event threshold ($\geq 0.5^\circ\text{C}$). If we use the zonal MSLP gradient to represent the Walker circulation (Fig. 12c), the main results are nearly unchanged except that the multimodel correlation between Niño-3.4 and the Walker circulation indicator becomes much larger than in Figs. 12a and 12b (0.84 vs 0.71, -0.55).

The diverse QBO–ENSO relationships in CMIP5/6 models are sensitive to the zonal position, intensity, and width of the detectable tropical convection, with the strongest impact associated with convection near the Maritime Continent (Indo-Pacific Ocean) and a weaker connection to convection or sea level pressure in the east Pacific in the reanalysis (Fig. 12). Overall, models are diverse in the QBO–ENSO linkage: ten models do not simulate a QBO–ENSO relationship (Figs. 11b,d–h,j–l,q), three simulate a negative relationship with a zonal shift of enhanced convection to the east of the Maritime Continent (Figs. 11c,m,r), and the other four simulate a positive relationship with enhanced convection over Indo-Pacific Ocean and weak downwelling over eastern Pacific (Figs. 11i,n–p). In the multimodel mean, there is little relationship between ENSO and the QBO.

7. Summary and discussion

a. Summary

The cycle period, composite amplitude, and the HT relationship of the QBO in the state-of-the-art CMIP5/6 models have been reported in a companion paper (Rao et al. 2020). As an extension to the previous results, this paper mainly focuses on the impact of the QBO on the tropospheric circulation by at least three dynamical pathways. The three dynamical pathways are 1) the NAM/AO response via the HT mechanism to impact the North Atlantic, Europe and the downstream regions (e.g., the Siberian high and East Asian winter monsoon; Thompson and Wallace 2000; Gong et al. 2001); 2) the equatorial stratospheric winds arching downward and poleward related to the direct meridional circulation cell response to the QBO (Garfinkel and Hartmann 2011a,b; Rao et al. 2020); and 3) the enhanced tropical convection associated with the cooling below the EQBO center and a decrease in static stability between the lower stratosphere and upper troposphere (Collimore et al. 2003; Liess and Geller 2012; Nie and Sobel 2015; Gray et al. 2018). The three pathways link the QBO and the tropospheric circulation in different regions. The first pathway is an important chain for the North Atlantic and European climate response to QBO, and then the projected NAM/AO influences other extratropical regions, especially the downstream areas. The second pathway bridges the tropical QBO forcing and the North Pacific circulation, and the projected change in the Aleutian low can impact the North Pacific and the downstream North American region. The third pathway probably links the

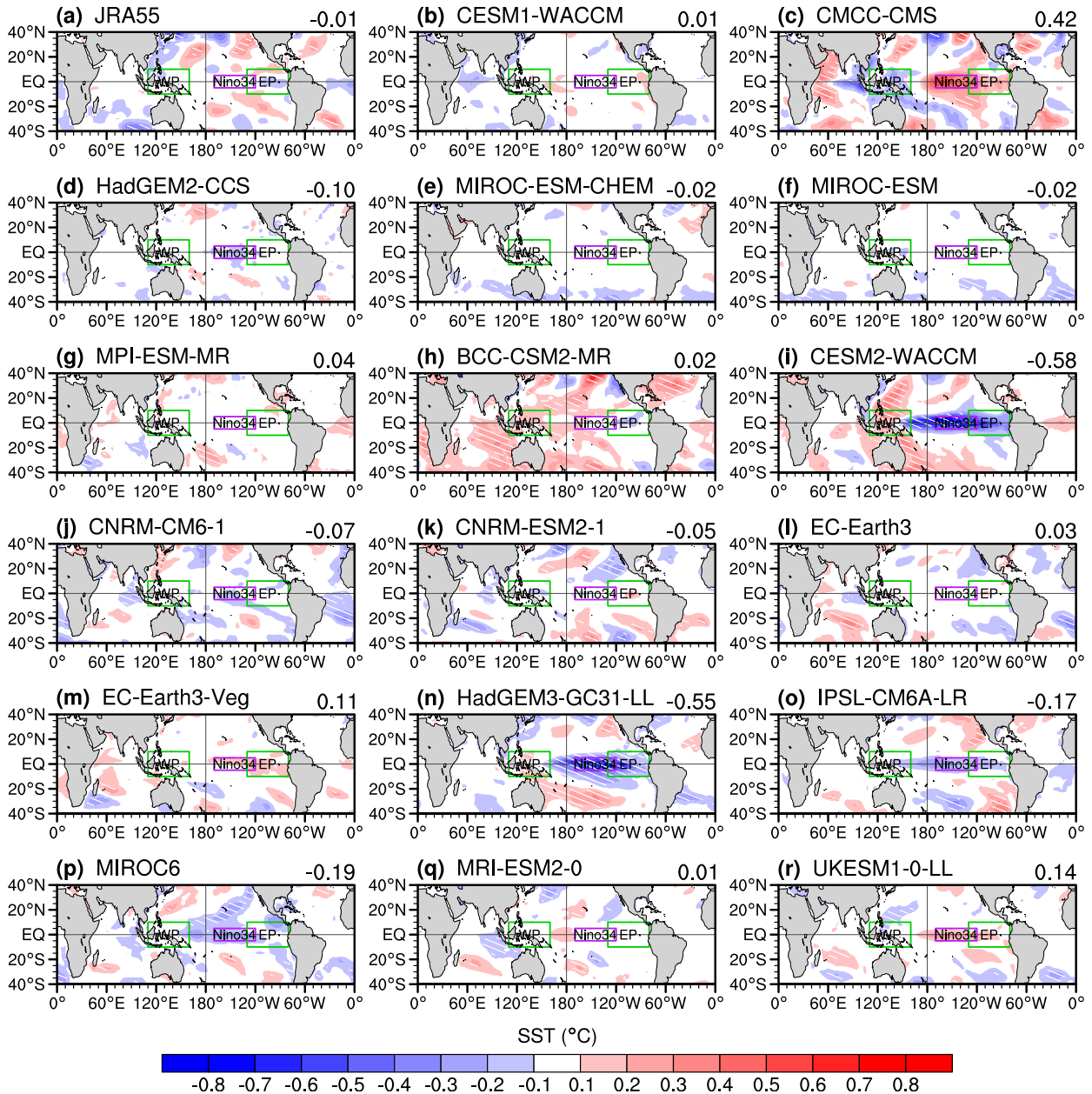


FIG. 11. Composite differences in the sea surface temperature (SST) anomalies (shadings; $^{\circ}\text{C}$) between EQBO and WQBO without the ENSO signal removed (i.e., the composite SST anomalies in the tropical Pacific are nearly zero in all datasets if the ENSO signal is removed) in the northern winter (December–February). The hatched regions mark the SST anomalies at the 90% confidence level according to Student's t test. The purple box marks the Niño-3.4 region, and the two green boxes mark the eastern and western Pacific. The area-weighted composite SST difference in the purple box is printed on the top right for each plot.

QBO forcing with the tropical troposphere and mainly affects the convection over Maritime Continent, where climatological convection is more active than elsewhere in the tropics. The tropical regions with less convection, especially those around the cold tongue, are not observed to have any detectable QBO signal in most models (although some models show significant convection anomalies outside the key region).

Very few CMIP5/6 models resolve all three pathways bridging the QBO winds and tropospheric circulation, and rather most models can only reproduce one or two of these routes. Furthermore, the complete chain for each pathway might break at some points in most models. To summarize the general performance of each model in simulating the three dynamical pathways, Fig. 13 shows key chains for the three dynamical pathways from the reanalysis and their simulations

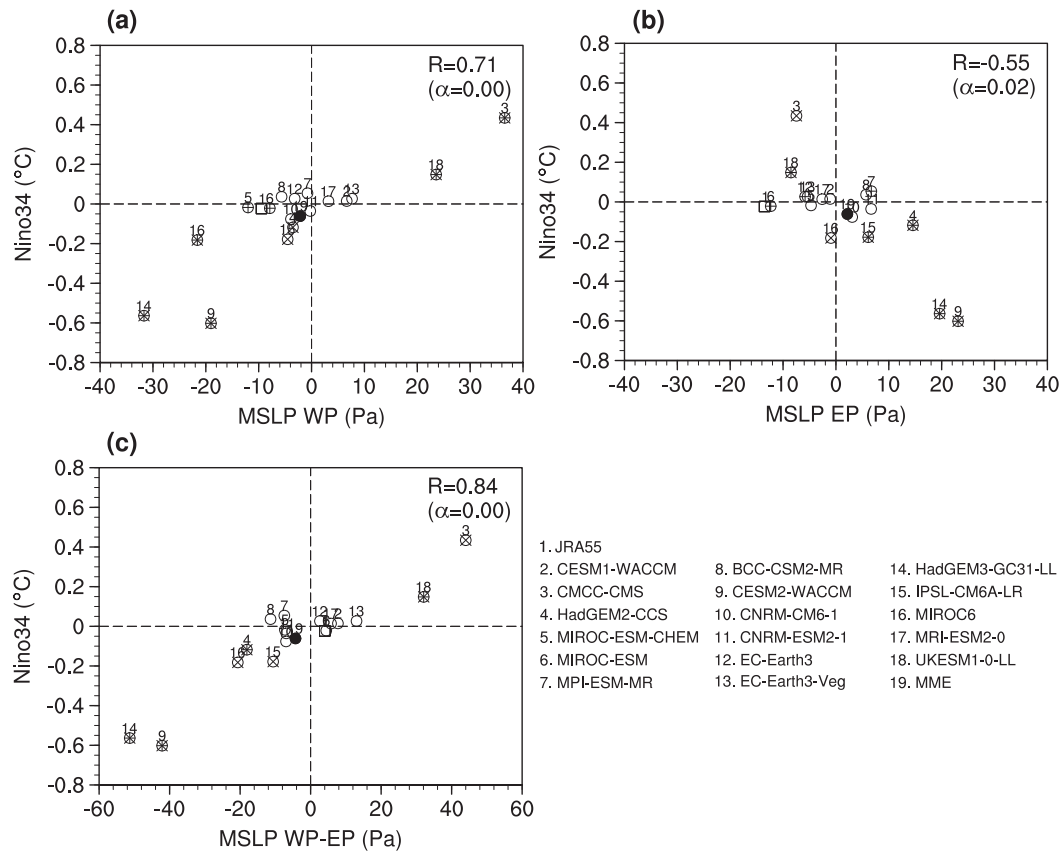


FIG. 12. Scatterplots of the composite winter-mean (December–February) sea level pressure (MSLP) difference between EQBO and WQBO (a) over the western Pacific (WP; 10°S–10°N, 110°–160°E), (b) over the eastern Pacific (EP; 10°S–10°N, 130°–80°W), and (c) their difference (WP – EP) vs the composite winter-mean (December–February) Niño-3.4 index (5°S–5°N, 170°–120°W) without the ENSO signal removed. The WP, EP, and Niño-3.4 regions are marked in Fig. 11. The circle (square) is shown for models (JRA-55), and a cross (plus) sign denotes the composite value of the y (x) axis at the 95% confidence level. The multimodel correlation (R) and its significance level (α) are also printed on the top-right corner of each plot.

in models. For the first pathway, similar to the reanalysis (gray cells), seven models (yellow and green cells) simulate a weak polar vortex during EQBO winters as the circumpolar westerlies are decelerated. These seven models also simulate a negative near-surface AO/NAO response (albeit quantitatively weaker than the reanalysis) in late winter during EQBO. In contrast, other models do not simulate the weak polar vortex response, and hence the chain between the stratospheric polar vortex and tropospheric NAM/AO is broken in these models (e.g., CESM1-WACCM, CMCC-CMS, HadGEM2-CCS, MPI-ESM-MR, BCC-CSM2-MR, CNRM-CM6.1, EC-Earth3-Veg, HadGEM3-GC31-LL, IPSL-CM6A-LR, MRI-ESM2.0). We find that the phasing of the QBO with respect to the seasonal cycle differs among these two classes of models, and can help explain the difference in tropospheric response.

The second pathway induced by the downward and poleward arching of QBO winds is also simulated with different degrees of similarity to the reanalysis. Ten models (e.g., CESM1-WACCM, CMCC-CMS, MIROC-ESM-CHEM, MIROC-ESM, BCC-CSM2-MR, CNRM-ESM2.1, EC-Earth3, IPSL-CM6A-LR,

MRI-ESM2.0, UKESM1.0-LL) simulate a different extratropical easterly anomaly center over 20°–40°N in the Pacific sector during EQBO, and the tropical tropospheric westerly anomalies in the Pacific sector is also not consistently simulated. The Pacific extratropical easterlies in the upper troposphere create negative relative velocity poleward of the easterly center, which explain a North Pacific high center ($v' \ll u'$, $\zeta = -\partial u'/\partial y \approx -\partial u'_g/\partial y \sim \partial^2 z'/\partial y^2 \sim -z'$). The inconsistently modeled height response over the North Pacific in those models is mainly caused by the difference in the wind anomaly amplitude, wind anomaly center, and wind anomaly meridional breadth (but insensitive to the choice of a QBO index in the lower stratosphere or using the phase 7 minus 3 composite). While the multimodel-mean downward-arching effect is much weaker than the observed effect (Fig. 5), some individual models simulate an effect stronger than that observed. The downward arching of QBO winds and creation of negative vorticity mainly explain the North Pacific circulation anomalies, whereas the stratospheric impact due to downward propagation of stratospheric polar vortex anomalies is

| Model or baseline | Pathway 1: HT mechanism and polar vortex | Pathway 2: QBO winds downward arching | Pathway 3: Tropical convection over Indo-Pacific Ocean | Statistical relationship between QBO and ENSO |
|-------------------|--|---|--|---|
| JRA55 (baseline) | EQBO → weak polar vortex → negative NAO | EQBO → locally negative vorticity → North Pacific high center | EQBO → enhanced convection → more rainfall and cold tropopause | Undetectable |
| CESM1-WACCM | | | | |
| CMCC-CMS | A shallow vortex response | | | Negative |
| HadGEM2-CCS | | | | |
| MIROC-ESM-CHEM | | | | |
| MIROC-ESM | | | | |
| MPI-ESM-MR | | | | |
| BCC-CSM2-MR | | | | |
| CESM2-WACCM | | | | Positive |
| CNRM-CM6-1 | | | | |
| CNRM-ESM2-1 | | | | |
| EC-Earth3 | | | | |
| EC-Earth3-Veg | | | | Negative but not robust |
| HadGEM3-GC31-LL | | | | Positive |
| IPSL-CM6A-LR | | | | Positive but not robust |
| MIROC6 | | | | Positive but not robust |
| MRI-ESM2-0 | | | Convection center shifted | |
| UKESM1-0-LL | | | | Negative but not robust |

FIG. 13. The evaluation of the three pathways for the QBO's impact on the troposphere and QBO–ENSO relationship in CMIP5/6 models, with the JRA-55 reanalysis (gray cells) as a baseline (three colors: red cells = little similarity between the specific model and the baseline; yellow cells = moderate similarity; green cells = high similarity). A comment might appear in the cell if the difference between the model and the baseline is evident. A positive QBO–ENSO relationship in the last column indicates that QBO30 and ENSO SST anomalies are of the same sign (easterly QBO and La Niña; westerly QBO and El Niño) or vice versa (easterly QBO and El Niño; westerly QBO and La Niña).

relatively weaker in this region as compared to the North Atlantic.

The third pathway is possibly related to deep convection over the Indo-Pacific Ocean, where a warm pool is situated. The QBO signal is mainly observed in the region with the strongest climatological convection, whereas the OLR, and precipitation anomalies are not detectable over cold tongue regions in the reanalysis. Seven models (e.g., CESM1-WACCM, HadGEM2-CCS, MIROC-ESM-CHEM, MIROC-ESM, MPI-

ESM-MR, BCC-CSM2-MR, IPSL-CM6A-LR) simulate enhanced convection associated with the EQBO over the Maritime Continent, although no response is evident in the multimodel mean (Fig. 7). Near-tropopause buoyancy frequency squared is found to discriminate between models that fail to simulate the observed effect and those that are more successful, with models that simulate enhanced Indo-Pacific Ocean convection for EQBO also simulating reduced near-tropopause buoyancy frequency squared, but with different anomaly amplitudes and

significance levels. A weak and insignificant intermodel relationship between Maritime Continent convection and the North Pacific height center during EQBO is also found, which might be related to the teleconnection spanning the tropics and extratropics. In contrast, the contribution by tropical convection to the North Pacific circulation in the multimodel ensemble mean is much less than that directly by downward arching QBO winds.

There is no direct connection between QBO and ENSO events in the JRA-55 reanalysis. Ten models show a similar lack of any relationship (e.g., CESM1-WACCM, HadGEM2-CCS, MIROC-ESM-CHEM, MIROC-ESM, MPI-ESM-MR, BCC-CSM2-MR, CNRM-CM6.1, CNRM-ESM2.1, EC-Earth3, MRI-ESM2.0), and while the other seven simulate a weak QBO–ENSO relationship, they disagree regarding the sign. A negative QBO and ENSO relationship is present in three models (CMCC-CMS, EC-Earth3-Veg, UKESM1.0-LL), whereas a positive QBO and ENSO relationship appears in four models (CESM2-WACCM, HadGEM3-GC31-LL, IPSL-CM6A-LR, MIROC6). The different QBO–ENSO relationship in CMIP models might be attributable to the widths, positions, and amplitudes of tropical enhanced convection and suppressed convection. Accordingly, no systematic Walker circulation anomaly is detected in the reanalysis and 10 models, together with no statistical relationship between QBO and ENSO. The enhanced convection center in three models is biased to middle and eastern Pacific (i.e., the climatological Walker circulation is perturbed), and hence El Niño-like SST anomalies appear in tropical Pacific. An organized active convection center over the Indo-Pacific Ocean and/or an inactive convection center over the eastern Pacific simultaneously form in four models (i.e., the climatological Walker circulation is strengthened), favoring a development of La Niña during EQBO winters. In the multimodel mean there is no connection between the QBO and ENSO.

b. Discussion

Using multiple CMIP5/6 models, the three dynamic pathways to connect QBO and the tropospheric response are systematically evaluated. It is expected that a comparison between models will provide us an opportunity to well understand the mechanism for tropospheric impact of QBO. In addition to these three pathways that are either directly or indirectly linked to the dynamical response to the QBO, some studies also emphasized the roles of radiative and/or chemical changes in response to the QBO. Through deep convection, the QBO has been shown to affect clouds and water vapor in the tropical upper troposphere in models (Randel et al. 1998; Giorgetta et al. 2002; Garfinkel and Hartmann 2011b; Kawatani et al. 2014; Nie and Sobel 2015) and observations (Liess and Geller 2012; Yoo and Son 2016). Some trace gases such as stratospheric water vapor (i.e., the “tape recorder” effect), aerosol, and ozone can be modulated by the QBO in their redistribution (Gray and Pyle 1987; Hitchman et al. 1994; Randel et al. 1998; Kawatani et al. 2014), so the balance in shortwave and longwave radiation is modified by changes in tracer concentrations. These physical and chemical pathways linking QBO and tropospheric variations in multiple models are beyond the scope of this study. Due to the lack of

interactive chemistry in some models, a parallel comparison of the contribution of ozone to the stratospheric variability is still difficult at the present stage of the CMIP.

Some previous studies (e.g., Huang et al. 2012; Hu et al. 2012) revealed the possible impact of the QBO on the development of ENSO events, but this QBO–ENSO relationship is not present in the reanalysis data, as well as in more than half of the evaluated models. The QBO has a cycle of around 28 months in observations and models, but ENSO has a much wider frequency width (2–7 years). The diagnosed weak QBO–ENSO relationship might mainly reflect the sample uncertainty and the natural variability to some extent. Specifically, the QBO index at 30 hPa is negatively correlated with the ENSO index before 1980s, whereas this correlation become positive after the 1980s (Domeisen et al. 2019). Such a change is consistent with the phase coincidence of QBO and ENSO phases: in pre-1980s data, El Niño events prefer EQBO rather than WQBO winds, and La Niña events prefer WQBO to EQBO winds; in post-1980s data, El Niño events tend to occur during WQBO, and La Niña events tend to occur during EQBO. However, if we use the entire JRA-55 reanalysis, no ENSO–QBO relationship can be established.

Most models do not show any significant relationship between ENSO and QBO, and the relationship in other models is also not of the same sign, as determined by the Walker circulation anomaly during QBO. The climatological Walker circulation consists of active convection over the Indo-Pacific Ocean and inactive convection over eastern Pacific, but the convection response to QBO is much narrower in the zonal direction. Because all the model datasets are from historical runs, much longer than the short reanalysis, the QBO–ENSO relationship in these models is likely not due to natural variability and sampling uncertainty. Any bias in the amplitude, width, and central position of the convection anomaly and in the frequency of ENSO in models might lead to an artificial QBO–ENSO relationship.

Our study mainly focuses on the interannual relationship between the QBO and tropospheric response, but some previous studies have also reported the possible modulation of the MJO by the QBO in northern winter (Yoo and Son 2016; Zhang and Zhang 2018). For example, it is estimated that 40% of interannual variability of the MJO in northern winter is explained by the QBO (e.g., Peña-Ortiz et al. 2019). Using satellite observations, Kim et al. (2018) found that the tropical convection warms the upper troposphere and cools the lower stratosphere, which in turn affects the static stability in the upper troposphere and lower stratosphere. However, we emphasize the impact of the QBO on the static stability on monthly and seasonal time scales and therefore tropical convection, although convective activities also affect the temperature and buoyancy variations. In addition, the easternmost position of the MJO convection is also different between EQBO and WQBO (farther eastward for the former with a larger amplitude) (Yoo and Son 2016; Son et al. 2017; Hendon and Abhik 2018; Zhang and Zhang 2018). A relatively weak tropical convection response to the QBO over Maritime Continent in the CMIP models as compared to observations may lead to an overly weak MJO convective response to the

QBO. The QBO–MJO relationship in CMIP5/6 models should be explored in future work.

Some CMIP5 and QBOi models have shown that the QBO cycle might shorten in a warmer future climate, but its amplitude is weakened (Kawatani and Hamilton 2013; Schirber et al. 2014; Richter et al. 2020). We still know little about the QBO changes and the impact of the QBO in the future based on CMIP6 models (Butchart et al. 2020). The CMIP6 database is still being filled, and the future scenario experiments are also gradually being uploaded for those models that can resolve the QBO. The projected changes in the intensity, cycle period, HT relationship (e.g., Butchart et al. 2020), and the three dynamical tropospheric pathways of the QBO are worthy of further investigation.

Acknowledgments. JR was funded by the National Key R&D Program of China (2016YFA0602104) and the National Natural Science Foundation of China (41705024). CIG, IW, and JR are also funded by the European Research Council starting grant under the European Union’s Horizon 2020 research and innovation programme (677756). We acknowledge the ESGF for providing historical runs from 17 CMIP5/6 models (<https://esgf-node.llnl.gov/projects/esgf-llnl/>). The JRA-55 reanalysis can be downloaded using FTP (https://jra.kishou.go.jp/JRA-55/index_en.html#download) after registration.

REFERENCES

- Andrews, M. B., J. R. Knight, A. A. Scaife, Y. Lu, T. Wu, L. J. Gray, and V. Schenzinger, 2019: Observed and simulated teleconnections between the stratospheric quasi-biennial oscillation and Northern Hemisphere winter atmospheric circulation. *J. Geophys. Res. Atmos.*, **124**, 1219–1232, <https://doi.org/10.1029/2018JD029368>.
- Anstey, J. A., and T. G. Shepherd, 2014: High-latitude influence of the quasi-biennial oscillation. *Quart. J. Roy. Meteor. Soc.*, **140** (678), 1–21, <https://doi.org/10.1002/qj.2132>.
- Baldwin, M. P., and K.-K. Tung, 1994: Extra-tropical QBO signals in angular-momentum and wave forcing. *Geophys. Res. Lett.*, **21**, 2717–2720, <https://doi.org/10.1029/94GL02119>.
- , and T. J. Dunkerton, 1999: Propagation of the Arctic Oscillation from the stratosphere to the troposphere. *J. Geophys. Res.*, **104**, 30 937–30 946, <https://doi.org/10.1029/1999JD900445>.
- , and Coauthors, 2001: The quasi-biennial oscillation. *Rev. Geophys.*, **39**, 179–229, <https://doi.org/10.1029/1999RG000073>.
- Bushell, A. C., and Coauthors, 2020: Evaluation of the Quasi-Biennial Oscillation in global climate models for the SPARC QBO initiative. *Quart. J. Roy. Meteor. Soc.*, <https://doi.org/10.1002/qj.3765>, in press.
- Butchart, N., and Coauthors, 2018: Overview of experiment design and comparison of models participating in phase 1 of the SPARC Quasi-Biennial Oscillation initiative (QBOi). *Geosci. Model Dev.*, **11**, 1009–1032, <https://doi.org/10.5194/gmd-11-1009-2018>.
- , J. A. Anstey, Y. Kawatani, S. Osprey, J. H. Richter, and T. Wu, 2020: QBO changes in CMIP6 climate projections. *Geophys. Res. Lett.*, **47**, e2019GL086903, <https://doi.org/10.1029/2019gl086903>.
- Calvo, N., and Coauthors, 2017: Northern Hemisphere stratospheric pathway of different El Niño flavors in stratosphere-resolving CMIP5 models. *J. Climate*, **30**, 4351–4371, <https://doi.org/10.1175/JCLI-D-16-0132.1>.
- Charlton-Perez, A. J., and Coauthors, 2013: On the lack of stratospheric dynamical variability in low-top versions of the CMIP5 models. *J. Geophys. Res. Atmos.*, **118**, 2494–2505, <https://doi.org/10.1002/jgrd.50125>.
- Collimore, C. C., D. W. Martin, M. H. Hitchman, A. Huesmann, and D. E. Waliser, 2003: On the relationship between the QBO and tropical deep convection. *J. Climate*, **16**, 2552–2568, [https://doi.org/10.1175/1520-0442\(2003\)016<2552:OTRBTQ>2.0.CO;2](https://doi.org/10.1175/1520-0442(2003)016<2552:OTRBTQ>2.0.CO;2).
- Crooks, S. A., and L. J. Gray, 2005: Characterization of the 11-year solar signal using a multiple regression analysis of the ERA-40 dataset. *J. Climate*, **18**, 996–1015, <https://doi.org/10.1175/JCLI-3308.1>.
- Davini, P., C. Cagnazzo, P. G. Fogli, E. Manzini, S. Gualdi, and A. Navarra, 2014: European blocking and Atlantic jet stream variability in the NCEP/NCAR reanalysis and the CMCC-CMS climate model. *Climate Dyn.*, **43**, 71–85, <https://doi.org/10.1007/s00382-013-1873-y>.
- Domeisen, D. I. V., C. I. Garfinkel, and A. H. Butler, 2019: The teleconnection of El Niño Southern Oscillation to the stratosphere. *Rev. Geophys.*, **57**, 5–47, <https://doi.org/10.1029/2018RG000596>.
- Dufresne, J. L., and Coauthors, 2013: Climate change projections using the IPSL-CM5 Earth system model: From CMIP3 to CMIP5. *Climate Dyn.*, **40**, 2123–2165, <https://doi.org/10.1007/s00382-012-1636-1>.
- Eyring, V., S. Bony, G. A. Meehl, C. A. Senior, B. Stevens, R. J. Stouffer, and K. E. Taylor, 2016: Overview of the Coupled Model Intercomparison Project Phase 6 (CMIP6) experimental design and organization. *Geosci. Model Dev.*, **9**, 1937–1958, <https://doi.org/10.5194/gmd-9-1937-2016>.
- Fletcher, C. G., and P. J. Kushner, 2011: The role of linear interference in the annular mode response to tropical SST forcing. *J. Climate*, **24**, 778–794, <https://doi.org/10.1175/2010JCLI3735.1>.
- Garfinkel, C. I., and D. L. Hartmann, 2007: Effects of the El Niño–Southern Oscillation and the Quasi-Biennial Oscillation on polar temperatures in the stratosphere. *J. Geophys. Res.*, **112**, D19112, <https://doi.org/10.1029/2007JD008481>.
- , and —, 2011a: The influence of the quasi-biennial oscillation on the troposphere in winter in a hierarchy of models. Part I: Simplified dry GCMs. *J. Atmos. Sci.*, **68**, 1273–1289, <https://doi.org/10.1175/2011JAS3665.1>.
- , and —, 2011b: The influence of the quasi-biennial oscillation on the troposphere in winter in a hierarchy of models. Part II: Perpetual winter WACCM runs. *J. Atmos. Sci.*, **68**, 2026–2041, <https://doi.org/10.1175/2011JAS3702.1>.
- , T. A. Shaw, D. L. Hartmann, and D. W. Waugh, 2012: Does the Holton–Tan mechanism explain how the quasi-biennial oscillation modulates the Arctic polar vortex? *J. Atmos. Sci.*, **69**, 1713–1733, <https://doi.org/10.1175/JAS-D-11-0209.1>.
- , C. Schwartz, D. I. Domeisen, S. W. Son, A. H. Butler, and I. P. White, 2018: Extratropical atmospheric predictability from the quasi-biennial oscillation in subseasonal forecast models. *J. Geophys. Res. Atmos.*, **123**, 7855–7866, <https://doi.org/10.1029/2018JD028724>.
- Giorgetta, M. A., E. Manzini, and E. Roeckner, 2002: Forcing of the quasi-biennial oscillation from a broad spectrum of atmospheric waves. *Geophys. Res. Lett.*, **29**, 1245, <https://doi.org/10.1029/2002GL014756>.
- , and Coauthors, 2013: Climate and carbon cycle changes from 1850 to 2100 in MPI-ESM simulations for the Coupled Model Intercomparison Project phase 5. *J. Adv. Model. Earth Syst.*, **5**, 572–597, <https://doi.org/10.1002/jame.20038>.

- Gong, D.-Y., S.-W. Wang, and J.-H. Zhu, 2001: East Asian winter monsoon and Arctic Oscillation. *Geophys. Res. Lett.*, **28**, 2073–2076, <https://doi.org/10.1029/2000GL012311>.
- Gray, L. J., and J. A. Pyle, 1987: Two-dimensional model studies of equatorial dynamics and tracer distributions. *Quart. J. Roy. Meteor. Soc.*, **113**, 635–651, <https://doi.org/10.1002/qj.49711347611>.
- , J. A. Anstey, Y. Kawatani, H. Lu, S. Osprey, and V. Schenzinger, 2018: Surface impacts of the quasi biennial oscillation. *Atmos. Chem. Phys.*, **18**, 8227–8247, <https://doi.org/10.5194/acp-18-8227-2018>.
- Haigh, J. D., M. Blackburn, and R. Day, 2005: The response of tropospheric circulation to perturbations in lower-stratospheric temperature. *J. Climate*, **18**, 3672–3685, <https://doi.org/10.1175/JCLI3472.1>.
- Hendon, H. H., and S. Abhik, 2018: Differences in vertical structure of the Madden–Julian oscillation associated with the quasi-biennial oscillation. *Geophys. Res. Lett.*, **45**, 4419–4428, <https://doi.org/10.1029/2018GL077207>.
- Hitchman, M. H., M. McKay, and C. R. Trepte, 1994: A climatology of stratospheric aerosol. *J. Geophys. Res.*, **99**, 20 689–20 700, <https://doi.org/10.1029/94JD01525>.
- Holton, J. R., and H. C. Tan, 1980: The Influence of the equatorial quasi-biennial oscillation on the global circulation at 50 mb. *J. Atmos. Sci.*, **37**, 2200–2208, [https://doi.org/10.1175/1520-0469\(1980\)037<2200:TIOTEQ>2.0.CO;2](https://doi.org/10.1175/1520-0469(1980)037<2200:TIOTEQ>2.0.CO;2).
- Hu, Z.-Z., B. Huang, J. L. Kinter, Z. Wu, and A. Kumar, 2012: Connection of the stratospheric QBO with global atmospheric general circulation and tropical SST. Part II: Interdecadal variations. *Climate Dyn.*, **38**, 25–43, <https://doi.org/10.1007/s00382-011-1073-6>.
- Huang, B., Z.-Z. Hu, J. L. Kinter, Z. Wu, and A. Kumar, 2012: Connection of stratospheric QBO with global atmospheric general circulation and tropical SST. Part I: Methodology and composite life cycle. *Climate Dyn.*, **38** (1–2), 1–23, <https://doi.org/10.1007/s00382-011-1250-7>.
- Hurwitz, M. M., N. Calvo, C. I. Garfinkel, A. H. Butler, S. Ineson, C. Cagnazzo, E. Manzini, and C. Peña-Ortiz, 2014: Extratropical atmospheric response to ENSO in the CMIP5 models. *Climate Dyn.*, **43**, 3367–3376, <https://doi.org/10.1007/s00382-014-2110-z>.
- Kawatani, Y., and K. Hamilton, 2013: Weakened stratospheric quasi-biennial oscillation driven by increased tropical mean upwelling. *Nature*, **497**, 478–481, <https://doi.org/10.1038/nature12140>.
- , J. N. Lee, and K. Hamilton, 2014: Interannual variations of stratospheric water vapor in MLS observations and climate model simulations. *J. Atmos. Sci.*, **71**, 4072–4085, <https://doi.org/10.1175/JAS-D-14-0164.1>.
- Kim, J., W. J. Randel, and T. Birner, 2018: Convectively driven tropopause-level cooling and its influences on stratospheric moisture. *J. Geophys. Res. Atmos.*, **123**, 590–606, <https://doi.org/10.1002/2017JD027080>.
- Kobayashi, S., and Coauthors, 2015: The JRA-55 reanalysis: General specifications and basic characteristics. *J. Meteor. Soc. Japan*, **93**, 5–48, <https://doi.org/10.2151/jmsj.2015-001>.
- Kuhlbrodt, T., and Coauthors, 2018: The low-resolution version of HadGEM3 GC3.1: Development and evaluation for global climate. *J. Adv. Model. Earth Syst.*, **10**, 2865–2888, <https://doi.org/10.1029/2018MS001370>.
- Li, F., Y. V. Vikhliav, P. A. Newman, S. Pawson, J. Perlwitz, D. W. Waugh, and A. R. Douglass, 2016: Impacts of interactive stratospheric chemistry on Antarctic and Southern Ocean climate change in the Goddard Earth Observing System, version 5 (GEOS-5). *J. Climate*, **29**, 3199–3218, <https://doi.org/10.1175/JCLI-D-15-0572.1>.
- Liess, S., and M. A. Geller, 2012: On the relationship between QBO and distribution of tropical deep convection. *J. Geophys. Res.*, **117**, D03108, <https://doi.org/10.1029/2011JD016317>.
- Liu, H.-L., and Coauthors, 2018: Development and validation of the Whole Atmosphere Community Climate Model with thermosphere and ionosphere extension (WACCM-X 2.0). *J. Adv. Model. Earth Syst.*, **10**, 381–402, <https://doi.org/10.1002/2017MS001232>.
- Lu, Y., T. Wu, W. Jie, A. A. Scaife, M. B. Andrews, and J. H. Richter, 2020: Variability of the stratospheric quasi-biennial oscillation and its wave forcing simulated in the Beijing Climate Center atmospheric general circulation model. *J. Atmos. Sci.*, **77**, 149–165, <https://doi.org/10.1175/JAS-D-19-0123.1>.
- Marsh, D. R., M. J. Mills, D. E. Kinnison, J. F. Lamarque, N. Calvo, and L. M. Polvani, 2013: Climate change from 1850 to 2005 simulated in CESM1(WACCM). *J. Climate*, **26**, 7372–7391, <https://doi.org/10.1175/JCLI-D-12-00558.1>.
- Marshall, A. G., and A. A. Scaife, 2009: Impact of the QBO on surface winter climate. *J. Geophys. Res.*, **114**, D18110, <https://doi.org/10.1029/2009JD011737>.
- Martin, G. M., and Coauthors, 2011: The HadGEM2 family of Met Office Unified Model climate configurations. *Geosci. Model Dev.*, **4**, 723–757, <https://doi.org/10.5194/gmd-4-723-2011>.
- Massonnet, F., M. Ménégoz, M. Acosta, X. Yepes-Arbós, E. Exarchou, and F. J. Doblas-Reyes, 2020: Replicability of the EC-Earth3 Earth system model under a change in computing environment. *Geosci. Model Dev.*, **13**, 1165–1178, <https://doi.org/10.5194/gmd-13-1165-2020>.
- Menary, M. B., and Coauthors, 2018: Preindustrial control simulations with HadGEM3-GC3.1 for CMIP6. *J. Adv. Model. Earth Syst.*, **10**, 3049–3075, <https://doi.org/10.1029/2018MS001495>.
- Naoe, H., and K. Yoshida, 2019: Influence of quasi-biennial oscillation on the boreal winter extratropical stratosphere in QBOi experiments. *Quart. J. Roy. Meteor. Soc.*, **145**, 2755–2771, <https://doi.org/10.1002/qj.3591>.
- Nie, J., and A. H. Sobel, 2015: Responses of tropical deep convection to the QBO: Cloud-resolving simulations. *J. Atmos. Sci.*, **72**, 3625–3638, <https://doi.org/10.1175/JAS-D-15-0035.1>.
- Peña-Ortiz, C., E. Manzini, and M. A. Giorgetta, 2019: Tropical deep convection impact on southern winter stationary waves and its modulation by the quasi-biennial oscillation. *J. Climate*, **32**, 7453–7467, <https://doi.org/10.1175/JCLI-D-18-0763.1>.
- Randel, W. J., F. Wu, J. M. Russell, A. Roche, and J. W. Waters, 1998: Seasonal cycles and QBO variations in stratospheric CH₄ and H₂O observed in UARS HALOE data. *J. Atmos. Sci.*, **55**, 163–185, [https://doi.org/10.1175/1520-0469\(1998\)055<0163:SCAQVI>2.0.CO;2](https://doi.org/10.1175/1520-0469(1998)055<0163:SCAQVI>2.0.CO;2).
- , —, R. Swinbank, J. Nash, and A. O'Neill, 1999: Global QBO circulation derived from UKMO stratospheric analyses. *J. Atmos. Sci.*, **56**, 457–474, [https://doi.org/10.1175/1520-0469\(1999\)056<0457:GQCDFU>2.0.CO;2](https://doi.org/10.1175/1520-0469(1999)056<0457:GQCDFU>2.0.CO;2).
- Rao, J., and R.-C. Ren, 2016: A decomposition of ENSO's impacts on the northern winter stratosphere: Competing effect of SST forcing in the tropical Indian Ocean. *Climate Dyn.*, **46**, 3689–3707, <https://doi.org/10.1007/s00382-015-2797-5>.
- , and —, 2018: Varying stratospheric responses to tropical Atlantic SST forcing from early to late winter. *Climate Dyn.*, **51**, 2079–2096, <https://doi.org/10.1007/s00382-017-3998-x>.
- , and —, 2020: Modeling study of the destructive interference between tropical Indian Ocean and eastern Pacific in their forcing in the southern winter extratropical stratosphere

- during ENSO. *Climate Dyn.*, **54**, 2249–2266, <https://doi.org/10.1007/s00382-019-05111-6>.
- , C. I. Garfinkel, and R. Ren, 2019: Modulation of the northern winter stratospheric El Niño–Southern Oscillation teleconnection by the PDO. *J. Climate*, **32**, 5761–5783, <https://doi.org/10.1175/JCLI-D-19-0087.1>.
- , —, and I. P. White, 2020: Impact of quasi-biennial oscillation on the northern winter stratospheric polar vortex in CMIP5/6 models. *J. Climate*, **33**, 4787–4813, <https://doi.org/10.1175/JCLI-D-19-0663.1>.
- Richter, J. H., A. Solomon, and J. T. Bacmeister, 2014: On the simulation of the quasi-biennial oscillation in the Community Atmosphere Model, version 5. *J. Geophys. Res. Atmos.*, **119**, 3045–3062, <https://doi.org/10.1002/2013JD021122>.
- , and Coauthors, 2020: Response of the quasi-biennial oscillation to a warming climate in global climate models. *Quart. J. Roy. Meteor. Soc.*, <https://doi.org/10.1002/qj.3749>, in press.
- Rind, D., J. Jonas, N. K. Balachandran, G. A. Schmidt, and J. Lean, 2014: The QBO in two GISS global climate models: 1. Generation of the QBO. *J. Geophys. Res. Atmos.*, **119**, 8798–8824, <https://doi.org/10.1002/2014JD021678>.
- Ruzmaikin, A., J. Feynman, X. Jiang, and Y. L. Yung, 2005: Extratropical signature of the quasi-biennial oscillation. *J. Geophys. Res.*, **110**, D11111, <https://doi.org/10.1029/2004JD005382>.
- Scaife, A. A., J. R. Knight, G. K. Vallis, and C. K. Folland, 2005: A stratospheric influence on the winter NAO and North Atlantic surface climate. *Geophys. Res. Lett.*, **32**, L18715, <https://doi.org/10.1029/2005GL023226>.
- Schirber, S., E. Manzini, T. Krismer, and M. Giorgetta, 2014: The quasi-biennial oscillation in a warmer climate: Sensitivity to different gravity wave parameterizations. *Climate Dyn.*, **45**, 825–836, <https://doi.org/10.1007/s00382-014-2314-2>.
- Séférian, R., and Coauthors, 2016: Development and evaluation of CNRM Earth system model—CNRM-ESM1. *Geosci. Model Dev.*, **9**, 1423–1453, <https://doi.org/10.5194/gmd-9-1423-2016>.
- Seo, J., W. Choi, D. Youn, D.-S. R. Park, and J. Y. Kim, 2013: Relationship between the stratospheric quasi-biennial oscillation and the spring rainfall in the western North Pacific. *Geophys. Res. Lett.*, **40**, 5949–5953, <https://doi.org/10.1002/2013GL058266>.
- Son, S.-W., Y. Lim, C. Yoo, H. H. Hendon, and J. Kim, 2017: Stratospheric control of the Madden–Julian oscillation. *J. Climate*, **30**, 1909–1922, <https://doi.org/10.1175/JCLI-D-16-0620.1>.
- Tatebe, H., and Coauthors, 2019: Description and basic evaluation of simulated mean state, internal variability, and climate sensitivity in MIROC6. *Geosci. Model Dev.*, **12**, 2727–2765, <https://doi.org/10.5194/gmd-12-2727-2019>.
- Taylor, K. E., R. J. Stouffer, and G. A. Meehl, 2012: An overview of CMIP5 and the experiment design. *Bull. Amer. Meteor. Soc.*, **93**, 485–498, <https://doi.org/10.1175/BAMS-D-11-00094.1>.
- Thompson, D. W. J., and J. M. Wallace, 2000: Annular modes in the extratropical circulation. Part I: Month-to-month variability. *J. Climate*, **13**, 1000–1016, [https://doi.org/10.1175/1520-0442\(2000\)013<1000:AMITEC>2.0.CO;2](https://doi.org/10.1175/1520-0442(2000)013<1000:AMITEC>2.0.CO;2).
- Voldoire, A., and Coauthors, 2019: Evaluation of CMIP6 DECK experiments with CNRM-CM6-1. *J. Adv. Model. Earth Syst.*, **11**, 2177–2213, <https://doi.org/10.1029/2019MS001683>.
- Watanabe, S., and Coauthors, 2011: MIROC-ESM 2010: Model description and basic results of CMIP5-20c3m experiments. *Geosci. Model Dev.*, **4**, 845–872, <https://doi.org/10.5194/gmd-4-845-2011>.
- Watson, P. A. G., and L. J. Gray, 2014: How does the quasi-biennial oscillation affect the stratospheric polar vortex? *J. Atmos. Sci.*, **71**, 391–409, <https://doi.org/10.1175/JAS-D-13-096.1>.
- White, I. P., H. Lu, N. J. Mitchell, and T. Phillips, 2015: Dynamical response to the QBO in the northern winter stratosphere: Signatures in wave forcing and eddy fluxes of potential vorticity. *J. Atmos. Sci.*, **72**, 4487–4507, <https://doi.org/10.1175/JAS-D-14-0358.1>.
- , —, and —, 2016: Seasonal evolution of the QBO-induced wave forcing and circulation anomalies in the northern winter stratosphere. *J. Geophys. Res. Atmos.*, **121**, 10 411–10 431, <https://doi.org/10.1002/2015JD024507>.
- Wu, T., and Coauthors, 2019: The Beijing Climate Center Climate System Model (BCC-CSM): The main progress from CMIP5 to CMIP6. *Geosci. Model Dev.*, **12**, 1573–1600, <https://doi.org/10.5194/gmd-12-1573-2019>.
- Yoo, C., and S.-W. Son, 2016: Modulation of the boreal wintertime Madden–Julian oscillation by the stratospheric quasi-biennial oscillation. *Geophys. Res. Lett.*, **43**, 1392–1398, <https://doi.org/10.1002/2016GL067762>.
- Yukimoto, S., and Coauthors, 2019: The Meteorological Research Institute Earth System Model version 2.0, MRI-ESM2.0: Description and basic evaluation of the physical component. *J. Meteor. Soc. Japan*, **97**, 931–965, <https://doi.org/10.2151/jmsj.2019-051>.
- Zhang, C., and B. Zhang, 2018: QBO–MJO connection. *J. Geophys. Res. Atmos.*, **123**, 2957–2967, <https://doi.org/10.1002/2017JD028171>.